# Chapter 14

# Falling Film Evaporation

(This chapter was updated in 2009.)

**Summary:** Horizontal, shell-side falling film evaporators have a significant potential to replace flooded evaporators in large refrigeration systems and also to be used in place of vertical tube-side falling evaporators in the petrochemical industry. The main advantages for the first application are higher heat transfer performance and reduced refrigerant charge. For petrochemical applications, shell-side falling film evaporation on horizontal tube bundles is advantageous because enhanced boiling tubes, such as the Turbo-Bii or Turbo-Biii, can be utilized and hence a much more compact design is obtained compared to vertical plain tube units. Additionally, such a unit can also take advantage of multiple tube passes for the heating fluid, further improving heat transfer performance and compactness.

In this chapter, the state-of-the-art of evaporation on horizontal single tubes and horizontal tube bundles is reviewed. Emphasis is placed on recent work on enhanced tubes. The effects of lubricating oils on thermal performance are also described and some test results presented. Numerous experimental tests have been made for plain, low fin and enhanced geometry tubes in the past decade, primarily for fluids such as water, refrigerants and ammonia. Based on these test data, enhanced tubes have demonstrated significant heat transfer augmentation for falling film evaporation on horizontal bundles with respect to plain tube units. In fact, some enhanced tubes demonstrate higher performance functioning with evaporating falling films than for their original pool boiling performance. Heat transfer design methods for horizontal units are presented and discussed as well as methods for predicting the film flow mode transitions between vertical tube rows (droplet, column and sheet) in horizontal bundles. No comprehensive design method is yet available, however. The relative benefits of horizontal falling film units compared to vertical intube units, and to a lesser extent to flooded evaporators, are addressed. Some remarks on liquid distributors and minimum overfeed rates are also presented.

## 14.1 INTRODUCTION TO FALLING FILM EVAPORATION

Falling film evaporation is a process controlled by two different heat transfer processes. First of all, thin film evaporation is a heat transfer mechanism controlled by conduction and/or convection across the film where phase change is at the interface and whose magnitude is directly related to the thickness of the film and whether or not the film is laminar or turbulent. If the heat flux is above that required for onset of nucleation (nearly always the case for enhanced boiling tubes), nucleate boiling is also present, where bubbles grow in the thin film at the heated wall (or in the re-entrant channels of an enhanced structured surface) and migrate to the interface. The film normally flows downward under the force of gravity. Therefore, except for the nucleate boiling mechanism, this process is quite similar to *falling film condensation* and in fact many analogies can be drawn between these two processes. For instance, falling film evaporation can occur in a laminar film flowing down the outside of a horizontal tube, similar to the Nusselt (1916) theory for laminar film condensation. In both cases, heat transfer is mainly dictated by film thickness. Furthermore, this film may develop surface waves or become turbulent, depending on the local film Reynolds number. On the contrary, a falling evaporating film often also has nucleate boiling occurring in it, which further increases the heat transfer coefficient. Furthermore, the formation of dry patches on the tube of an evaporating film may occur, which is very detrimental to heat transfer since heat transfer is then only to the vapor-phase on those parts of the surface.

Figure 14.1 shows a schematic illustration of falling film evaporation on a single horizontal tube, with nucleate boiling occurring in the falling film. Hence, both thin falling film evaporation and nucleate

boiling play a role in the heat transfer process. In a falling film evaporator, an array of horizontal tubes arranged in a matrix is used with the liquid falling from tube to tube.

Vertical falling film evaporators have been used for many years in the petrochemical industry. As evidence, Kern (1950) included the design method of Bays and McAdams (1937) for vertical intube units in his widely used book. In the chemical industry, vertical falling film evaporators are utilized to evaporate fluids under vacuum conditions where the liquid static head from the distillation column would otherwise create too much subcooling for efficient operation as a vertical or horizontal thermosyphon reboiler. They are also used to evaporate temperature sensitive fluids and to remove volatiles from mixtures. The falling liquid film is placed on the tube-side of these vertical, plain tube exchangers so that uniform liquid distribution to the tubes on the top tubesheet can achieved by placing liquid distributor caps on each tube hole. The flow rate of liquid is controlled so as to inundate the tubes with liquid but rather to form a uniformly distributed falling liquid film inside each tube. Hence, it is *very* important to install these units with a strict tolerance to the vertical plumb line since a small inclination would result in dryout at the lower end of the tubes on the *higher* side.

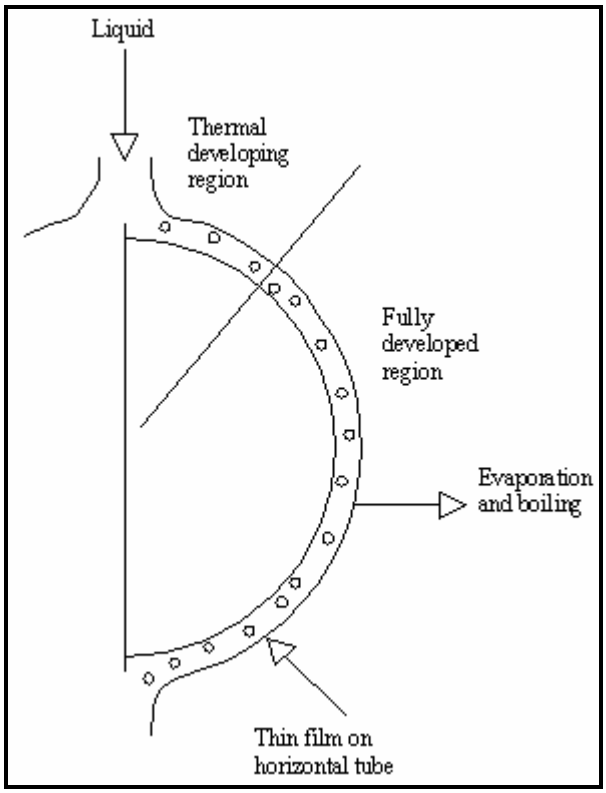


**Figure 14.1. Falling film evaporation on a heated horizontal tube with nucleate boiling.**

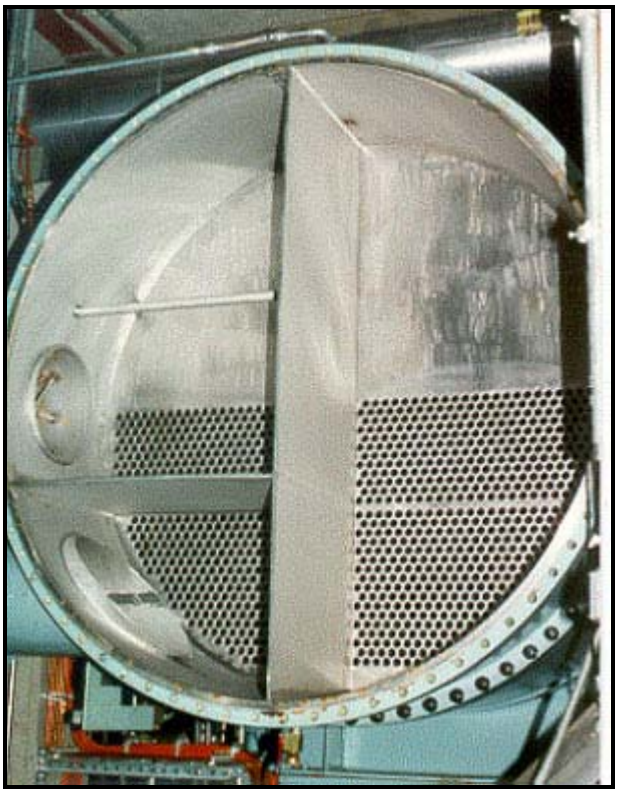

**Figure 14.2. Ammonia falling film evaporator at EPFL (view of head and tube sheet).**

Falling film evaporation has also been used on the shell-side of large heat pump systems. For example, an ammonia-cycle heat pump system at the Swiss Federal Institute of Technology in Lausanne (EPFL) takes thermal energy from Lake Geneva for central heating of the campus buildings, utilizing two 2 m diameter and 10 m long, horizontal shell-and-tube units that function with a significant amount of immiscible lubricating oil in the working fluid (refer to Figure 14.2). The desalination industry also exploits falling film evaporators, typically utilizing plain, horizontal tube bundles. This allows for closer temperature approaches and very significant energy savings. In large tonnage air-separation plants, massive vertical coiled-tube-in-shell units with shell-side falling film evaporation are used to take advantage of the close

temperature approaches that can be attained to save on energy consumption. Here the tubes are nearly horizontal in their spiral within the coil. Falling film evaporators have also been tested in Ocean Thermal Energy Conversion (OTEC) pilot plants, again to achieve a closer temperature approach between the evaporating fluid and the heating fluid, and hence attain higher cycle thermal efficiency. Falling film evaporation has also been exploited in absorbers and vapor generators of absorption heat pump systems. Falling film evaporators are also sometimes referred to as spray-film evaporators.

With respect to large refrigeration systems, one major U.S. refrigeration company brought out a complete new line of refrigeration units operating with R-134a at the beginning of 1998 based on enhanced tube falling film evaporators, achieving significant performance improvements compared to traditional enhanced tube flooded evaporators. A company in Texas has experience in using an inhouse enhanced tube for ammonia falling film evaporators since about 1992.

One of the significant advantages of falling film operation is the large reduction in liquid charge in the evaporator. Furthermore, higher heat transfer performance can also be attained. Also, for falling film evaporators applied to refrigeration units, the bottom tube rows can be purposely flooded to evaporate the access liquid reaching the bottom of the bundle and thus minimize the liquid that must be pumped back to the inlet. Horizontal falling film evaporators are to some extent similar to kettle-type steam generators in that the liquid is fed to the bundle overhead, using sprinklers or trays. The difference is that to achieve a falling film, the liquid holdup in the shell is reduced to a minimum and the liquid flow rate is limited to that required to wet the entire bundle without the formation of dry patches, rather than flooding the shell in a pool of liquid. The unevaporated liquid can be removed from the bottom of the bundle by placing a nozzle at the bottom of the shell as shown in Figure 14.3.

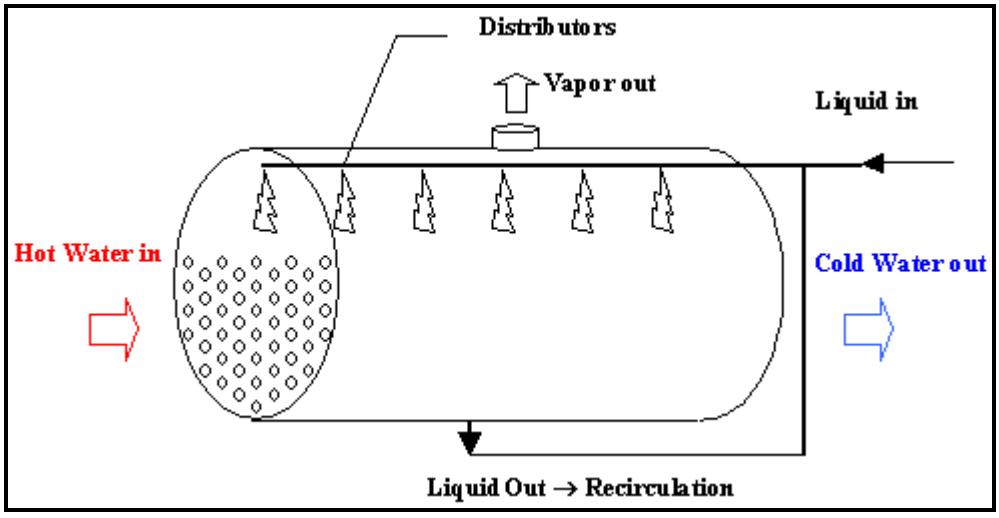


**Figure 14.3. A horizontal shell-and-tube falling film evaporator.**

## 14.2 AN ASSESSMENT OF ADVANTAGES/DISADVANTAGES

Before looking at the scientific details of falling film evaporation, let's first consider their overall attributes. Comparing horizontal falling film evaporators to flooded evaporators, the former have the following ***potential benefits***:

- Reduction in working fluid to about 1/3 that of a comparable flooded unit;
- Higher heat transfer performance;

- More uniformity in the overall U within the bundle;
- Closer temperature approach in some cases;
- More compact evaporator design;
- Improved oil removal (oil holds up in a flooded bundle but drains to the bottom of a falling film unit).

Comparing horizontal falling film evaporators to flooded evaporators, the former also have ***potential disadvantages***:

- Less design experience with falling film units;
- Uniformity of liquid distribution onto the top tube row;
- Less tolerance for undercharging of refrigerant to the unit.

For petrochemical applications, the ***potential advantages*** of using horizontal falling film units as opposed to vertical units can be summarized as follows:

- Heat transfer coefficients on plain horizontal tubes are higher than those for vertical tubes since the heated flow length is much shorter;
- External enhancements are available for tubes in copper, copper-nickel, carbon and stainless steels, etc. for up to a 10-fold increase in boiling coefficients;
- The temperature approach between the evaporating fluid and the heating fluid can be reduced to an absolute minimum for maximum thermal efficiency;
- A horizontal bundle can have multiple tube passes of the heating fluid to significantly increase its heat transfer coefficient compared to a single shell pass in vertical units;
- Longer, smaller diameter horizontal shell-and-tube units can be designed rather than short, large diameter shells often required in vertical units to avoid dryout and flooding in the tubes;
- Two-pass floating head (or even U-tube) designs can be specified in the horizontal units, which are much more convenient to maintain and cheaper than one-pass floating heads in vertical units;
- The reduced flow length of the liquid film minimizes the liquid holdup and residence time of temperature sensitive fluids;
- A horizontal orientation reduces the height of the liquid nozzle inlet with respect to grade and hence may reduce the amount of piping and the required elevation of the distillation column with respect to the top of the exchanger.

The principal disadvantage of horizontal units is for corrosive applications where alloy tubes are needed, which would mean placing the corrosive fluid on the shell-side. However, on the shell-side an enhanced surface may be applicable, which would greatly reduce the size of the unit with the potential of being more economical. In some materials, including carbon steel and copper-nickel alloys, doubly-enhanced tubes with internal helical ribs are available for augmenting the heating fluid side of horizontal falling film evaporators while little experience is available in using internal helically ribbed tubes for falling film evaporation in vertical units.

## 14.3 THERMAL DESIGN CONSIDERATIONS

Before looking at the state-of-the-art of falling film heat transfer, let's first consider what special aspects must be taken into account when designing a horizontal falling film evaporator. Indeed, much less experience and know how is generally available for designing horizontal falling film evaporators and thus ***new challenges*** face thermal designers, such as:

- Choice of the most appropriate enhanced tube for the fluid to be handled. Note that conventional low finned tubes should *not* be used since they tend to inhibit longitudinal spreading of the liquid film along the tube. On the other hand, enhanced pool boiling tubes and also enhanced falling film condensation tubes perform very well in the falling film evaporation mode.
- Choice of the optimum tube bundle layout (number of tubes and their length, bundle width and height, tube pitch and layout and number of tube passes). Optimizing the bundle size depends significantly on all these factors.
- Selection and proper placement of the spray nozzles or sprinklers or distribution trays to achieve uniform liquid distribution on the top row of tubes in the bundle. These systems are not readily available and most likely the designer will have to come up with his own solution.
- Minimum liquid overfeed necessary for proper operation of the unit. This involves avoiding the formation of dry patches (very low thermal performance) while at the same time limiting the flow rate of the liquid on the top of the bundle. Normally, the intertube flow mode between tubes should be sheet mode or staggered column mode, with the second one requiring a lower flow rate to achieve. The minimum liquid feed rate is hence that which still gives the staggered column mode on the lowest tube row.
- Vapor escape from the bundle. The tube layout should include a consideration of how to best facilitate the escape of vapor from the bundle.
- Local modeling of the heat transfer coefficients and mass transfer effects (important if the fluid is a zeotropic mixture) plus the influence of viscous components on performance, such as a lubricating oil in a refrigeration system;
- Proper oil separation in the liquid pool beneath the bundle in refrigeration evaporators to avoid oil builds up in the unit.

These points would also be relevant if designing a horizontal falling film evaporator in place of a horizontal flooded evaporator, a kettle reboiler, or a horizontal thermosyphon reboiler for petrochemical applications. In summary, there are numerous aspects to be considered and not all of them well understood, and some of them can only be resolved with experimental tests on prototype units.

There are also various ***thermal mechanisms*** and ***flow phenomena*** specific to falling film evaporation on horizontal tube bundles that must be kept in mind during thermal design:

- prediction of liquid film flow mode transitions between tubes;
- vapor shear effects on the liquid film flow in a tube bundle;
- crossflow effects of vapor flow on film flow modes between tubes;
- nucleate boiling in the film and its onset;
- prediction of heat transfer coefficients by tube row and intertube flow regime;
- prediction of the onset of dry patch formation;
- critical heat flux for nucleate boiling in thin films;
- effect of enhancement geometry on the above processes;
- effect of lubricating oil on the above processes.

All of these have an important influence on proper operation of these units and their thermal optimization, and essentially all require further study (in particular for fluids other than water and refrigerants).

## 14.4 INTERTUBE FALLING FILM MODES

Before discussing the research work on falling film evaporation heat transfer, it is instructive to first review the literature on the prediction of intertube falling film modes for plain and enhanced tubes. Figure

14.4 shows photographs of the five flow modes. The intertube flow modes are classified from observations as follows:

A. **Droplet mode.** The flow is in droplet mode when there is only a flow of liquid in the form of distinct droplets between the tubes.

B. **Droplet-Columns mode**. This intermediate mode is present when at least one stable column exists between the tubes in addition to falling droplets. A column is a continuous liquid link between tubes. A column can move horizontally along the tubes but has to be continuous to define this mode.

C. **Column mode.** This mode is simply when there is only liquid flow in columns between the tubes. At lower flow rates in this mode the columns tend to be *inline* while at higher flow rates they are *staggered* from one tube to the next.

D. **Column-Sheet mode**. In this intermediate mode, both columns and a liquid sheet are simultaneously flowing between the tubes at different locations along the tubes. It is reached when at least one small sheet is visible. This small sheet is formed by the merging of two nearby columns and typically has a triangular profile.

E. **Sheet mode**. This mode is when the fluid flows uniformly between the tubes as a continuous film or sheet.

The flow progresses from mode A to mode E as the mass flow rate is increased. There is normally some hysteresis in these transitions when observing them for increasing and decreasing flow rates. For practical purposes, it is probably best to ignore this secondary effect on thermal design.

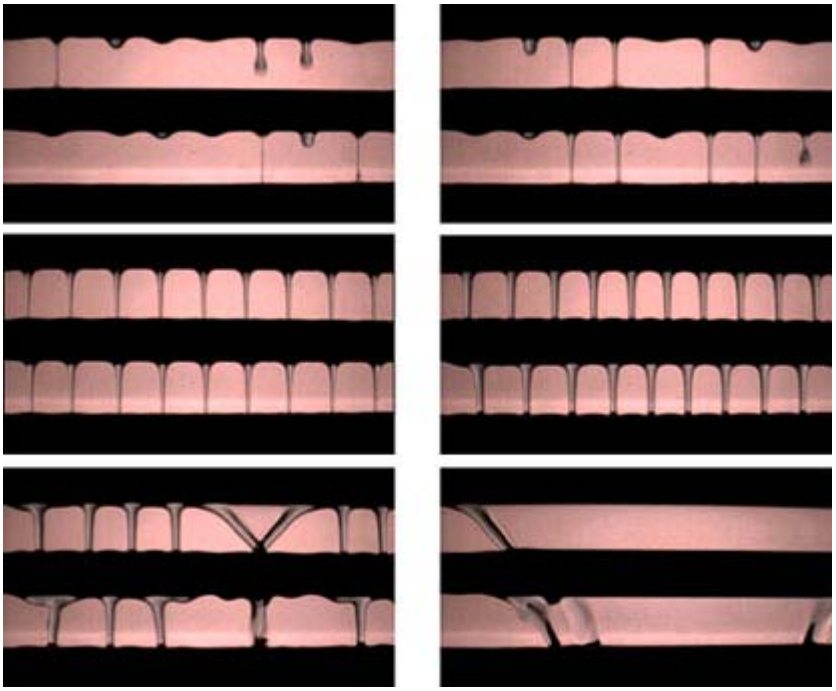

**Figure 14.4. Photographs of flow modes on plain tubes (from left to right, top to bottom): droplet, droplet-column, column (inline), column (staggered), column-sheet, and sheet.**

Despite numerous observations of condensation and falling film evaporation on rows of tubes, apparently no generalized flow mode map is currently available, although Honda et al. (1987) have made some transition expressions for individual fluids condensing on low finned tubes. These processes however are similar to adiabatic falling films of liquid fed onto the top of a tube array, which has been studied extensively by Hu and Jacobi (1996a) for a variety of fluids, tube diameters, tube pitches and flow rates and with/without cocurrent gas flow. Based on their observations, they proposed a flow mode map with coordinates of film Reynolds number versus modified Galileo number, $Re_\Gamma$ vs. $Ga_L$. The mixed mode zones of column-sheet and droplet-column are transition zones between the three dominant modes of sheet, column and droplet in which both modes are present. Their four flow transition expressions, between these five zones, are given below (valid for passing through the transitions in either direction and hence the symbol ⇔):

Droplet⇔Droplet-Column: $$Re_\Gamma = 0.074 Ga_L^{0.302}$$ [14.4.1]

Droplet-Column⇔Column: $$Re_\Gamma = 0.096 Ga_L^{0.301}$$ [14.4.2]

Column⇔Column-Sheet: $$Re_\Gamma = 1.414 Ga_L^{0.233}$$ [14.4.3]

Column-Sheet⇔Sheet: $$Re_\Gamma = 1.448 Ga_L^{0.236}$$ [14.4.4]

The modified Galileo number $Ga_L$ is defined as

$$Ga_L = \frac{\rho_L \sigma^3}{\mu_L^4 g}$$ [14.4.5]

The film Reynolds number $Re_\Gamma$ is defined in these transition equations as

$$Re_\Gamma = \frac{4\Gamma_L}{\mu_L}$$ [14.4.6]

where $\Gamma_L$ is the flow rate of liquid on one side of the tube per unit length of tube in kg/ms, so that the total flow rate on both sides of the tube is $2\Gamma_L$. This definition is consistent with $Re_\Gamma$ for a vertical plate where the flow rate in the film is $\Gamma_L$. Their map is applicable to plain tubes for air velocities less than 15 m/s. The modified Galileo number is sometimes referred to as the "film number" and is in fact the inverse of the Kapitza number, Ka, which is defined as

$$Ka = \frac{g\mu_L^4}{\rho_L \sigma^3}$$ [14.4.7]

Figure 14.5 of Roques, Dupont and Thome (2002) shows their flow mode transition map for an array of smooth 19.05 mm tubes obtained with observations for water, glycol and a 50%/50% water/glycol mixture. Their transition curves were quite similar to those reported earlier by Hu and Jacobi (1996a).

Figure 14.6 of Roques, Dupont and Thome (2002) gives their comparison of the transition boundaries obtained for the Turbo-Bii tube versus a plain, smooth tube of the same size. The primary difference is an enlargement of the zone in which column mode exists; that is, the column to column-sheet transition

occurs at higher film Reynolds numbers while the column to droplet-column transition occurs at lower $Re_\Gamma$. In practice, this means that an evaporating falling film will tend to stay in the advantageous column mode down to lower overfeed rates on Turbo-Bii tubes than on an array of plain tubes.

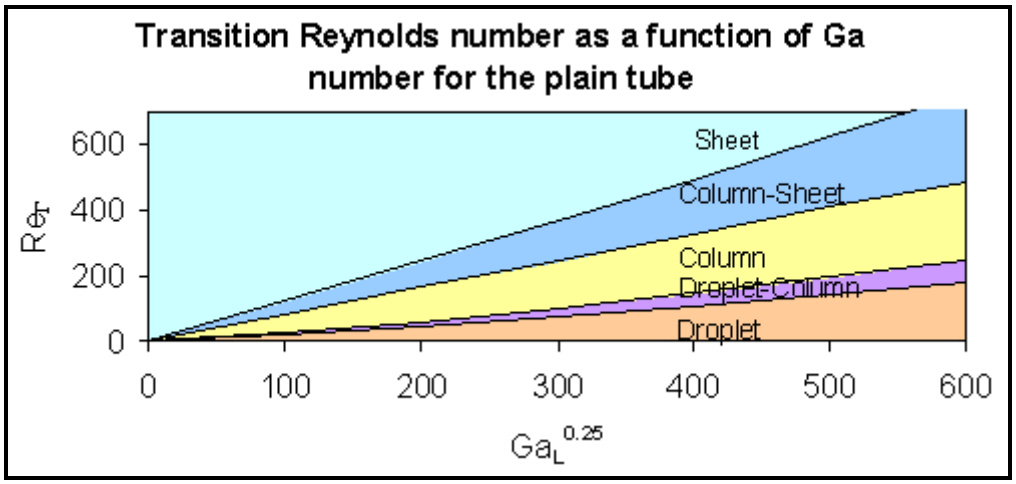


**Figure 14.5. Flow mode transition map for plain tubes.**

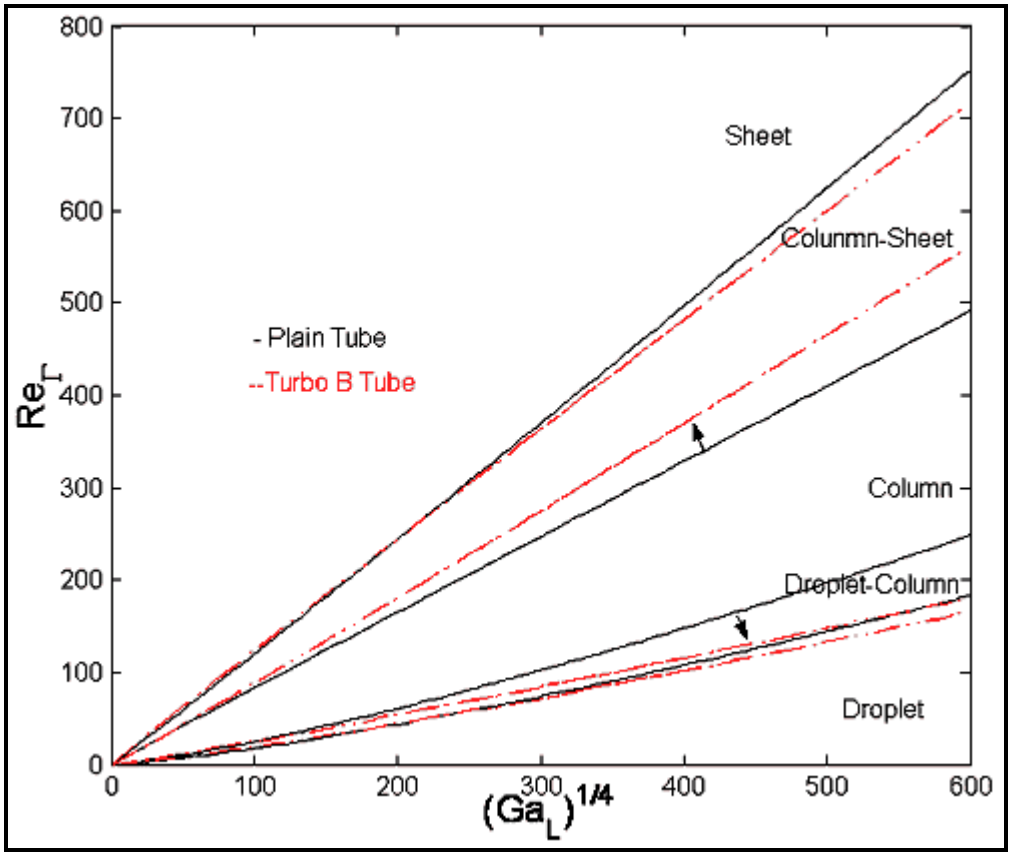


**Figure 14.6. Flow mode transition map for the Wolverine Turbo-Bii enhanced boiling tube.**

Figure 14.7 of Roques, Dupont and Thome (2002) shows a similar flow mode transition map for the 26 fpi Wolverine Turbo-Chil low finned tube versus a plain, smooth tube of the same size (note that low finned tubes are *not* recommended for falling film evaporation, however). Again, the primary difference is an enlargement of the zone in which column mode exists; that is, the column to column-sheet transition occurs at much higher film Reynolds numbers while the column to droplet-column transition occurs at somewhat lower $Re_\Gamma$. Roques and Thome (2002) have also presented transition expressions for 19 fpi and 40 fpi low finned tubes.

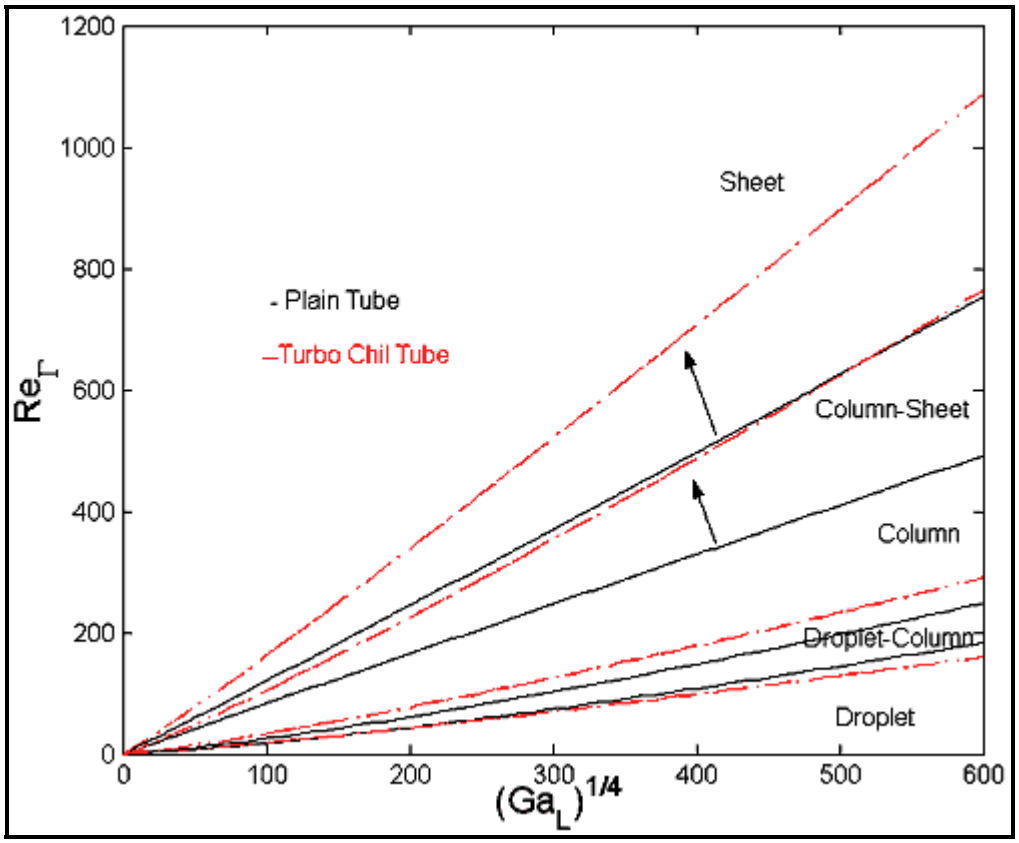


**Figure 14.7. Flow mode transition map for the Wolverine Turbo-Chil low fin tube.**

Since enhanced condensation tubes have been found experimentally to have significant performances when used for falling film evaporation, Figure 14.8 of Roques (2004) presents a flow mode transition map for the Wolverine Turbo-CSL tube. The primary difference relative to the plain tube array is an enlargement of the zone in which column mode exists; that is, the column to column-sheet transition occurs at much higher film Reynolds numbers while the column to droplet-column transition occurs at much lower $Re_\Gamma$.

The transition flow measurements and observations of Roques, Dupont and Thome (2002) have been correlated with the following expression

$$Re_\Gamma = a\, Ga_L^b \qquad [14.4.8]$$

The values of the coefficients *a* and *b* are listed in Table 14.1 for various tubes taken from the Thome and coworkers tests. The values can be compared to those of Hu and Jacobi (1996a) for plain tubes, which

give rather similar transition values considering the difficult in determining exactly where the transition occurs because of the subjectivity of visual observations.

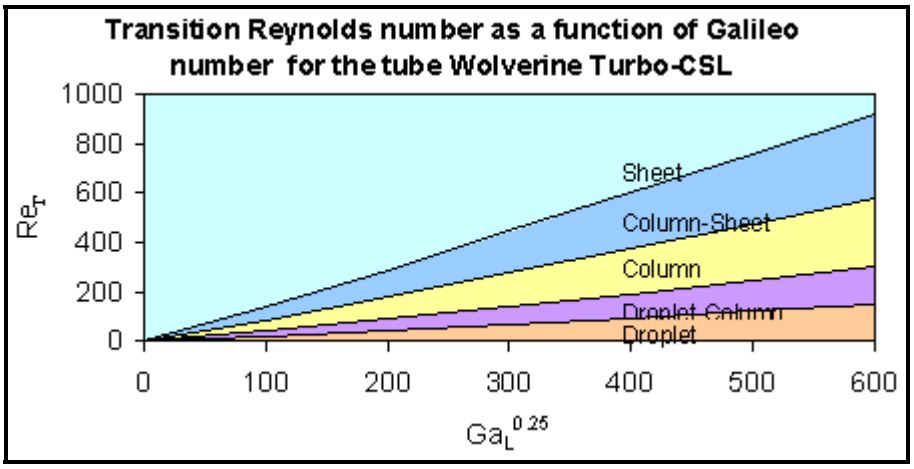


**Figure 14.8. Flow mode transition map for the Wolverine Turbo-CSL enhanced condensing tube.**

Earlier, Honda, Nozu and Takeda (1987) presented the transition expressions for their observations on a 27 fpi low finned tube of 15.9 mm (5/8 in.) diameter for R-113, methanol and n-propanol. Note that low finned tubes are not appropriate for falling film evaporators and this information is only given for comparison purposes to plain and other enhanced tubes. They gave transitions from droplet to column mode (ignoring the intermediate mode of droplet-column) and from column to column-sheet as follows:

Droplet⇔Column (for n-propanol): $$\mathrm{Re}_\Gamma = 0.244\mathrm{Ga}_L^{0.25} \quad [14.4.9]$$

Droplet⇔Column (for R-113): $$\mathrm{Re}_\Gamma = 0.52\mathrm{Ga}_L^{0.25} \quad [14.4.10]$$

Column⇔Column-Sheet (all 3 liquids): $$\mathrm{Re}_\Gamma = 1.28\mathrm{Ga}_L^{0.25} \quad [14.4.11]$$

Column-Sheet⇔Sheet (all 3 liquids): $$\mathrm{Re}_\Gamma = (1.48\,\text{to}\,1.88)\mathrm{Ga}_L^{0.236} \quad [14.4.12]$$

The last two expressions predict transitions similar to those found by Roques, Dupont and Thome (2002) for their 26 fpi low finned tube.

Hu and Jacobi (1998) have studied the horizontal distance between droplets and between columns in those respective flow modes, looking at the effect of intertube spacing of the tubes. More recently, Wei and Jacobi (2002) have investigated the effects of vapor-shear, tube diameter, tube spacing and bundle depth of the flow mode transitions. They observed that upflow of gas counter-current to the liquid flow tends to destablize the sheet and column modes. Tube spacing effects become important to mode transition thresholds, especially for (S-D)/Ca < 6 where S is the vertical tube pitch, D is the tube diameter and Ca is the capillary constant

$$\mathrm{Ca} = \left(\frac{\sigma}{g\rho_L}\right)^{1/2} \quad [14.4.13]$$

Regarding tube row effects, they observed that the flow generally became less stable farther down into the bundle from the top. This tended to eliminate the hysteresis effect on the transitions but also raised some of the transition film Reynolds numbers to higher values.

**Table 14.1. Coefficients for flow mode transitions for a selection of tubes.**

| Tube | Transition | a | b |
|---|---|---|---|
| **Plain** | Droplet to/from Droplet-Columns | 0.0417 | 0.3278 |
| | Droplet-Columns to/from Columns | 0.0683 | 0.3204 |
| | Columns to/from Columns-Sheet | 0.8553 | 0.2483 |
| | Columns-Sheet to/from Sheet | 1.068 | 0.2563 |
| **Low Fin (19fpi)** | Droplet to/from Droplet-Columns | 0.0827 | 0.3048 |
| | Droplet-Columns to/from Columns | 0.1217 | 0.3041 |
| | Columns to/from Columns-Sheet | 0.8573 | 0.2589 |
| | Columns-Sheet to/from Sheet | 1.3557 | 0.2532 |
| **Low Fin (26fpi)** | Droplet to/from Droplet-Columns | 0.0743 | 0.3000 |
| | Droplet-Columns to/from Columns | 0.1263 | 0.3025 |
| | Columns to/from Columns-Sheet | 0.6172 | 0.2783 |
| | Columns-Sheet to/from Sheet | 1.2015 | 0.2661 |
| **Low Fin (40fpi)** | Droplet to/from Droplet-Columns | 0.0622 | 0.3087 |
| | Droplet-Columns to/from Columns | 0.1148 | 0.2947 |
| | Columns to/from Columns-Sheet | 0.7198 | 0.2553 |
| | Columns-Sheet to/from Sheet | 0.9414 | 0.2662 |
| **Turbo-BII HP** | Droplet to/from Droplet-Columns | 0.0754 | 0.3007 |
| | Droplet-Columns to/from Columns | 0.1594 | 0.2748 |
| | Columns to/from Columns-Sheet | 0.7591 | 0.2482 |
| | Columns-Sheet to/from Sheet | 1.3487 | 0.2453 |
| **Thermo-excel-E** | Droplet to/from Droplet-Columns | 0.0975 | 0.2514 |
| | Droplet-Columns to/from Columns | 0.2293 | 0.2451 |
| | Columns to/from Columns-Sheet | 0.8146 | 0.2602 |
| | Columns-Sheet to/from Sheet | 1.5859 | 0.2561 |
| **Turbo-CSL** | Droplet to/from Droplet-Columns | 0.0690 | 0.3010 |
| | Droplet-Columns to/from Columns | 0.2380 | 0.2799 |
| | Columns to/from Columns-Sheet | 0.6686 | 0.2642 |
| | Columns-Sheet to/from Sheet | 1.1310 | 0.2620 |

## 14.5 HIGHLIGHTS OF HEAT TRANSFER STUDIES PRIOR TO 1994

No comprehensive review on falling film evaporation has appeared in recent years nor has any review provided a complete summary of the various design methods that have been proposed. In view of this fact, first the important publications prior to 1994 will be surveyed, where most of the research was on plain tubes and for fluids such as water or since retired refrigerants like R-11. After this, a more comprehensive review of publications since 1994 will be given. At the same time, a selection of the best design methods for horizontal units will also be presented, which at present are limited to pure fluids and thus require eventual extension to mixtures. Regarding prior reviews, Chyu and Bergles (1987) presented a well-written discussion on the effects of film flow rate, liquid feed height, and wall superheat on evaporation of falling films on plain tubes. Cerza (1992) summarized the nucleate boiling mechanisms occurring in thin falling films, paying particular attention to nucleation and rewetting of dry patches. Also, Thome (1999) presented an earlier version of the present review.

In a landmark paper of those presented before 1994, Chun and Seban (1971) reported falling film heat transfer coefficients for water on a vertical plain tube, in both laminar flow and turbulent flow regimes. In the laminar regime, they noted that heat is transferred by conduction across the falling liquid film according to the expression

$$h_{LG}\frac{d\Gamma_L}{dz}=k_L\frac{T_w-T_{sat}}{\delta} \qquad [14.5.1]$$

This is the same assumption assumed by Nusselt (1916) in his classic theory on falling film condensation. The mass flow rate per unit width of the wall $\Gamma_L$ in the above expression is modeled to be

$$\Gamma_L=\frac{g\rho_L^2\delta^3}{3\mu_L} \qquad [14.5.2]$$

Also relevant, Kapitza [cf. Dukler (1960)] predicted the formation of capillary waves on the interface of a falling laminar film when the film Reynolds number exceeded some critical value of the Kapitza number, Ka. Other criteria for the onset of interfacial waves on falling condensing films are presented in Chapter 7.

For film flow with interfacial waves, Chun and Seban (1971) estimated that the reduction in the average film thickness by the ripples was responsible for the increase in heat transfer they observed experimentally. They then presented the following empirical equations for predicting laminar and turbulent heat transfer in evaporating films on vertical tubes without nucleate boiling, respectively, in the fully developed region:

$$\alpha_{\Gamma,lam}=0.821\left(\frac{\mu_L^2}{g\rho_L^2k_L^3}\right)^{-0.333}Re_\Gamma^{-0.22} \qquad [14.5.3]$$

$$\alpha_{\Gamma,turb}=0.00381\left(\frac{\mu_L^2}{g\rho_L^2k_L^3}\right)^{-0.333}Re_\Gamma^{0.4}\left(\frac{\nu_L}{a_L}\right)^{0.65} \qquad [14.5.4]$$

where the film Reynolds number is

$$Re_{\Gamma} = \frac{4\Gamma_L}{\mu_L} \qquad [14.5.5]$$

Chun and Seban (1971) further suggested that the Weber number is a good parameter for predicting the transition from laminar to turbulent flow in falling films, defined as

$$We = \left( \frac{\rho_L u_L^2}{\sigma} \right)^{1/2} \qquad [14.5.6]$$

They proposed a transition criterion with We = 1. Fletcher et al. (1974) later experimentally studied falling film evaporation also for water, but on a horizontal plain tube using a liquid distributor system along its axis.

In one of the most comprehensive falling film evaporation studies to date on horizontal, plain tube bundles, Danilova et al. (1976) tested R-12, R-22 and R-113 on simulated bundles up to 40 rows deep. They tested 330 mm long, electrically heated stainless steel tubes of 18 mm O.D. with a 0.3 mm wall and nominal surface roughness of 1 micron. Their tubes were arranged in a tube bundle, utilizing the top tube for liquid distribution onto the lower tubes. Staggered tube bundles from one to three rows wide and six tube rows deep were tested with vertical tube pitch to tube diameter ratios of 1.1, 1.3, 1.5 and 2.2. Rather than reporting film *mass* flow rate per unit length of one side of the tube in kg/(m s), i.e. $\Gamma_L$, they have reported their data as *volumetric* flow rates per unit length of tube in $m^3/(m\ s)$. Figure 14.9 shows some of their results for R-22 in which three distinct heat transfer zones are evident:

1. In the film evaporation zone, the heat transfer coefficient is controlled by the liquid volumetric flow rate and is almost independent of heat flux q and saturation temperature $T_{sat}$;
2. In the developed boiling zone, the heat transfer coefficient is controlled by q and $T_{sat}$ but is nearly independent of liquid volumetric flow rate;
3. In the transition zone between the above to regimes, the heat transfer coefficient is affected by all three factors.

(a)

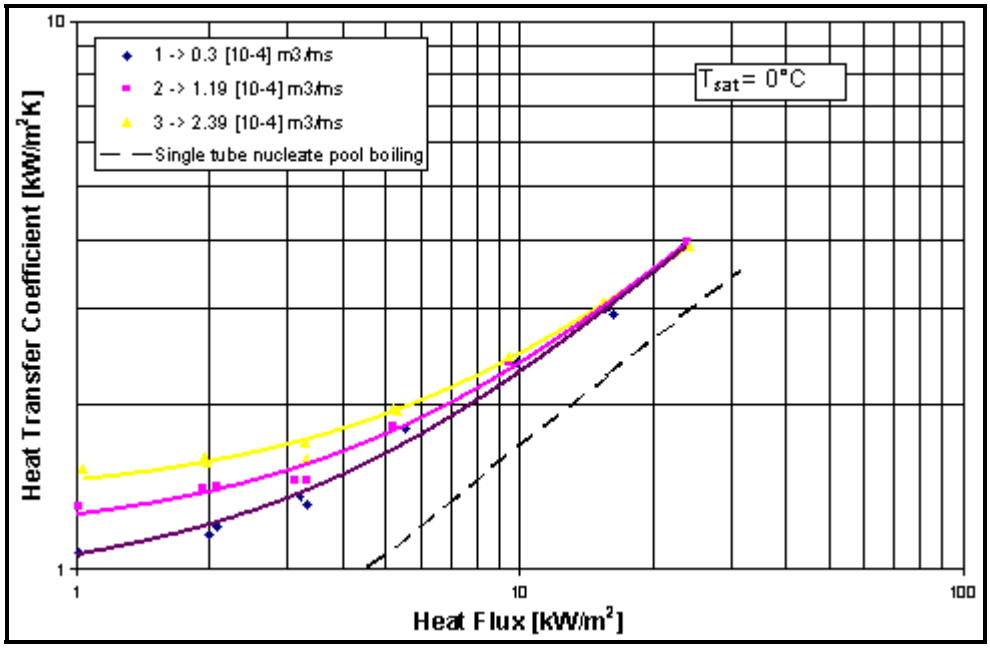

(b)

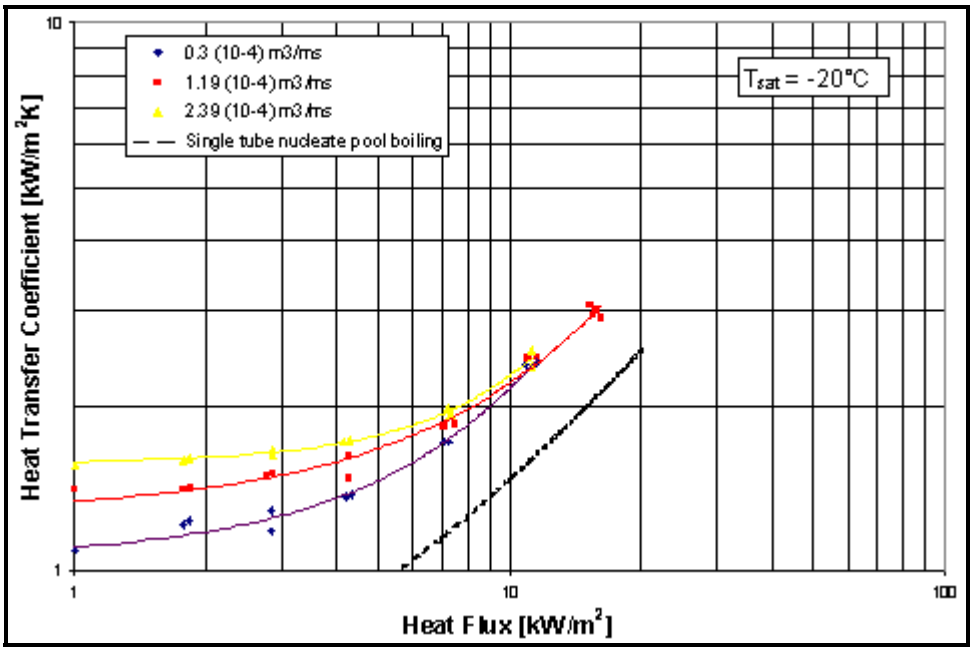


(c)

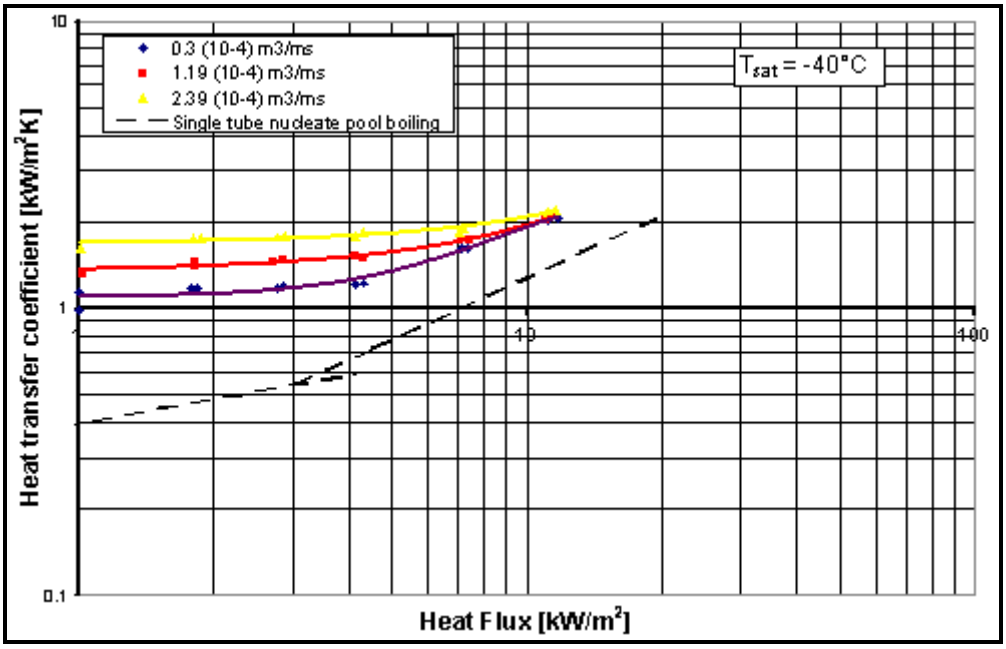


**Figure 14.9. Average heat transfer coefficients for R-22 for a selection of film flow rates compared to nucleate pool boiling from Danilova et al. (1976). Legend: $T_{sat}$ for (a) 0°C, (b) -20°C and (c) -40°C while volumetric flow rates per unit length were (1) 0.3x10$^{-4}$ m$^3$/(m s), (2) 1.19x10$^{-4}$ m$^3$/(m s) and (3) 2.39x10$^{-4}$ m$^3$/(m s). The dashed lines depict single-tube nucleate pool boiling curves.**

Based on these test results, they proposed an empirical correlation for film vaporization as a function of liquid film Reynolds number, liquid Prandtl number and the ratio of vertical tube pitch to tube diameter (S/D) and a second one for nucleate boiling. For film evaporation, all their data were correlated as a film Nusselt number:

$$Nu_{\Gamma} = 0.03\,Re_{\Gamma}^{0.22}\,Re_{*\Gamma}^{0.04}\,Pr_{L}^{0.32}\left(\frac{S}{D}\right) \qquad [14.5.7]$$

For nucleate boiling, the corresponding nucleate boiling Nusselt number is:

$$Nu_{nb} = 0.00132\,Re_{nb}^{0.63}\,K_{p}^{0.72}\,Pr_{L}^{0.48} \qquad [14.5.8]$$

Equation [14.5.5] is used for the film Reynolds number and $Pr_L$ is the liquid Prandlt number. The dimensionless numbers they used are defined below:

$$Nu_{\Gamma} = \frac{\alpha_{\Gamma}}{k_L}\left(\frac{\mu_L^2}{g\rho_L^2}\right)^{0.333} \qquad [14.5.9]$$

$$Nu_{nb} = \frac{\alpha_{\Gamma}}{k_L}\left(\frac{\sigma}{g(\rho_L - \rho_G)}\right)^{0.5} \qquad [14.5.10]$$

$$Re_{*\Gamma} = \frac{q\rho_L}{h_{LG}\rho_G\mu_L}\left(\frac{\mu_L^2}{g\rho_L^2}\right)^{0.333} \qquad [14.5.11]$$

$$Re_{nb} = \frac{q\rho_L}{h_{LG}\rho_G\mu_L}\left(\frac{\sigma}{g(\rho_L - \rho_G)}\right)^{0.5} \qquad [14.5.12]$$

$$K_p = \frac{p_{sat}}{\sigma}\left(\frac{\sigma}{g(\rho_L - \rho_G)}\right)^{0.5} \qquad [14.5.13]$$

Choosing the larger of these two values as the correct one, the maximum experimental deviation of their test points from these equations did not exceed ±15%.

Lorenz and Yung (1978, 1979) developed a combined model for film evaporation and nucleate boiling in liquid films flowing over a single, horizontal plain tube of circumferential length L, where L was set equal to the entire perimeter, i.e. L = πD. They considered three heating modes: that of a subcooled film over length $L_{dev}$, evaporation of a saturated film over the remaining length and nucleate boiling in the film over the entire perimeter. The mean heat transfer coefficient $\alpha_{mean}$ on the tube perimeter is the sum of these three individual contributions:

$$\alpha_{mean} = \alpha_{nb} + \alpha_{\Gamma,dev}\left(\frac{L_{dev}}{L}\right) + \alpha_{\Gamma}\left(1 - \frac{L_{dev}}{L}\right) \qquad [14.5.14]$$

where $\alpha_{nb}$ is the nucleate boiling coefficient over the entire length L, $\alpha_{\Gamma,dev}$ is the convective film heat transfer in the thermally developing region of length $L_{dev}$, and $\alpha_{\Gamma}$ is the convective film coefficient in the fully developed region given by either Equation [14.5.3] or [14.5.4] of Chun and Seban (1971) for vertical tubes. The developing region convective film heat transfer coefficient is for the initial subcooled zone

where the film is heated up to the saturation temperature of the liquid, and was derived based on simple heat conduction across the liquid film, such that

$$\alpha_{\Gamma,dev} = 0.375 c_{pL}\left(\frac{\Gamma_L}{L_{dev}}\right) \qquad [14.5.15]$$

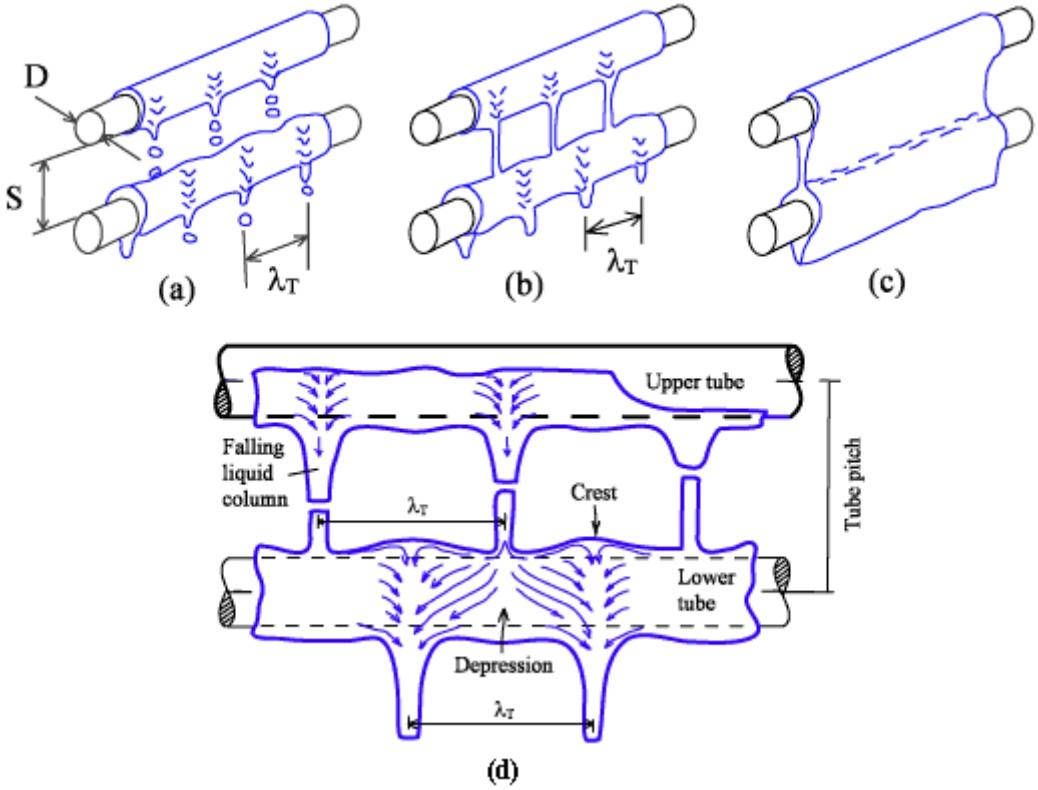


**Figure 14.10. Liquid falling film in (a) droplet mode, (b) in stable column mode, (c) in sheet mode and (d) the Taylor instability of vapor/liquid interface beneath a horizontal tube in staggered column mode.**

Continuing this work, Yung et al. (1980) investigated the effects of vapor/liquid interactions on the mode of liquid film flow off the bottom of horizontal tubes plus that of liquid entrainment caused by vapor crossflow in plain horizontal tube bundles. Notably, they presented a criterion for the transition from the liquid droplet mode to the column flow mode from one tube row to the next, similar to process occurring during intertube drainage of condensation on vertical tube rows, which is illustrated in Figure 14.10. They observed that the Taylor instability wave most likely to occur on the liquid interface underneath the tube has a wavelength $\lambda_T$:

$$\lambda_T = 2\pi\left(\frac{n\sigma}{g\rho_L}\right)^{1/2} \qquad [14.5.16]$$

The constant n in this expression is equal to 3 if the liquid film is relatively thick (thick film Taylor wavelength) or is equal to 2 if the liquid film is relatively thin (thin film Taylor wavelength). The value of 2 gave good agreement to their observations. For predicting the transition to column flow mode in Figure

14.10(b) from droplet mode in Figure 14.10(a), they predicted that this occurred at film flow rate per unit length of tube equal to:

$$\Gamma_{L,trans} = \left(\frac{0.81\pi\rho_L d_p^3}{6\lambda_T}\right)\left(\frac{2\pi\sigma}{\rho_L\lambda_T^3}\right)^{1/2} \qquad [14.5.17]$$

The primary droplet diameter $d_p$ is given by the following equation where the best constant found to match their observations was 3.0:

$$d_p = 3\left(\frac{\sigma}{g\rho_L}\right)^{1/2} \qquad [14.5.18]$$

Consequently, there was now a second method for predicting local heat transfer coefficients on horizontal tubes and a criterion for predicting one of the intertube film flow mode transitions.

To account for the effect of liquid feed height above a horizontal tube on falling film evaporation, Owens (1978) proposed several correlations based on his data and that of another two studies for evaporating falling films without nucleate boiling. For laminar films, he proposed:

$$Nu_{\Gamma,lam} = 2.2\left(\frac{H}{D}\right)^{0.1} Re_\Gamma^{1/3} \qquad [14.5.19]$$

For turbulent films, he proposed:

$$Nu_{\Gamma,turb} = 0.185\left(\frac{H}{D}\right)^{0.1} Re_\Gamma^{1/2} \qquad [14.5.20]$$

where H is the liquid feed height above the top of the tube and D is the tube diameter. The transition between these two flow regimes was predicted to occur when:

$$Re_{\Gamma,trans} = 1680\,Pr_L^{0.5} \qquad [14.5.21]$$

where the film Reynolds number $Re_\Gamma$ as defined in Equation [14.5.5]. This criterion is surprisingly a function of the liquid Prandtl number.

Nakayama et al. (1982) made a comparative experimental study, measuring falling film heat transfer coefficients for a vertical plate with a Hitachi Thermoexcel-E type of enhanced pool boiling surface, a vertical surface with vertically cut grooves and a vertical surface with horizontally cut grooves, all tested with R-11. The Thermoexcel-E type of surface promoted nucleate boiling on the plate, giving the best heat transfer performance, whose heat transfer coefficients in the falling film mode were larger than those for the pool boiling conditions. The horizontal grooves on the third plate promoted liquid holdup on the plate, i.e. thicker films, and hence yielded lower thermal performance than the plate with vertical grooves.

Chyu et al. (1982) measured falling film heat transfer coefficients for water on a horizontal plain tube, a UOP High Flux porous coated tube and a Wieland Gewa-T tube. The High Flux tube has a thin porous metallic coating to promote nucleate boiling while the Gewa-T geometry has characteristic T-shaped fins.

Both greatly outperformed the plain tube. Chyu and Bergles (1985a, 1987) later presented a method for predicting falling film coefficients on a plain, horizontal tube by zone. As illustrated in Figure 14.11, the perimeter of the tube was divided up into the following regions: stagnation flow at the top, an impingement flow region near the top, a thermally developing flow region, and finally a fully developed flow region around the rest of the tube. Their method is not presented here because it involves a numerical solution. In addition, Chyu and Bergles (1985b, 1989) reported falling film coefficients for water for four tubes: a Wieland Gewa-T tube, a Hitachi Thermoexcel-E tube, a UOP High Flux tube and a plain tube. The optimum type of geometry was found to depend on whether there was nucleate boiling in the film (favoring the High Flux and Thermoexcel-E geometries) or only film evaporation (which favored the Gewa-T's fins for thinning the liquid film).

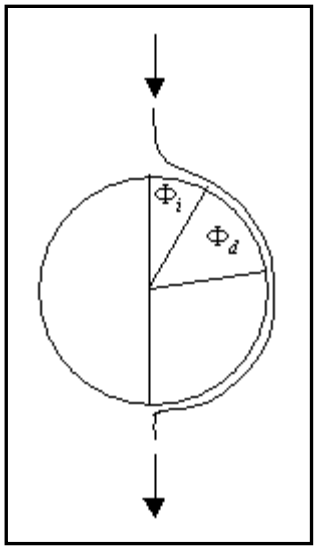


**Figure 14.11. Model of Chyu and Bergles (1985a) for falling film evaporation on a horizontal tube.**

The influence of intertube spacing and flow rate on falling film heat transfer on horizontal plain tube bundles for subcooled liquid without evaporation was investigated by Mitrovic (1986) for iso-propanol and water. Figure 14.10 depicts the flow pattern modes between two adjacent horizontal tubes in a vertical row that they observed: discrete droplet flow, liquid column flow and laminar or turbulent sheet flow. Figure 14.10(d) shows the flow structure for stationary liquid columns with flow from the top to bottom tube. A crest in the liquid film is also formed between the columns at the top of the tube when the columns are staggered as shown. Mitrovic measured the distance between the columns from still photographs, obtaining a value of 22 mm for water at 25°C and 13.5 mm for iso-propanol at 21.5°C, noting that these values fell between the critical wavelength $\lambda_{crit}$ and the most dangerous wavelength $\lambda_d$ calculated according to the following equations of Lienhard and Wong (1964):

$$\lambda_{crit} = 2\pi\left(\frac{g(\rho_L - \rho_G)}{\sigma} + \frac{2}{D^2}\right)^{-1/2} \qquad [14.5.22]$$

$$\lambda_d = \sqrt{3}\,\lambda_{crit} \qquad [14.5.23]$$

Similar values of wavelengths between liquid columns were also reported by Yung et al. (1980). For subcooled, non-evaporating liquid flows, Mitrovic proposed the following correlation for heat transfer where the Nusselt number of the liquid film $Nu_\Gamma$ is defined as in Equation [14.5.9] while the film Reynolds number is defined in the standard way by Equation [14.5.5] rather than using Mitrovic's definition of $\Gamma_L/\mu_L$:

$$Nu_\Gamma = 0.0175\left(\frac{Re_\Gamma}{4}\right)^{0.349} Pr_L^{0.5}\,\Omega \qquad [14.5.24]$$

His tube spacing correction factor Ω is based on the vertical tube pitch to tube diameter ratio (S/D) as:

$$\Omega = \frac{(S/D)^{0.158}}{1+\exp\left[-0.008\left(\frac{Re_\Gamma}{4}\right)^{1.32}\right]} \qquad [14.5.25]$$

Parken et al. (1990) measured local coefficients for both the nucleate boiling and film evaporation regimes around horizontal, plain brass tubes of 2.54 mm and 5.08 mm diameter as a function of angle. Non-boiling subcooled heat transfer coefficients tended to decrease sharply from the top of the tube to an angle of about 90° and then either continue to fall off more gradually or level off for the rest of the perimeter towards the bottom of the tube. Some data even showed a slight secondary maximum at 180° from the top, i.e. right at the bottom. Instead, the variation in local heat transfer around the tube was more complex for evaporating flows with some local nucleate boiling in the film and was not necessarily symmetric on both sides of the horizontal tubes. Rather than presenting general correlations, they presented separate methods for each size of tube.

Cerza (1992) surveyed previous studies with particular attention to the mechanisms of nucleate boiling in thin falling films. He identified the following ***influential parameters*** on the heat transfer process:

- Waves or ripples on the film interface;
- Heat flux (for onset of nucleation and nucleate boiling);
- Thermal entrance length for heating the film to the saturation temperature;
- Thermally fully developed length;
- Fluid-surface wettability (dry patch formation);
- Nucleate site distribution.

Rifert et al. (1992) reported falling film coefficients for a plain tube and horizontal tubes with longitudinally grooves in a vertical tube row of six tubes for water. This gave about 1.4 to 1.9 heat transfer augmentation factors for the grooves.

## 14.6 HEAT TRANSFER STUDIES SINCE 1994

These more recent heat transfer studies are described below, more or less in chronological order. These investigations have covered a very broad range of geometries for horizontal falling film evaporation: plain tubes, enhanced tubes, oil effects, intertube flow mode effects on subcooled films, tube layout effects, tube diameter effects, types of sprayers, etc.

Fujita and Tsutsui (1994) obtained R-11 falling film heat transfer coefficients at a pressure of 0.2 MPa for a vertical array of plain, horizontal tubes of 25 mm diameter with a 50 mm vertical tube pitch. They observed the following intertube flow modes of the falling films from tube to tube: discrete droplets, droplets, columns, disturbed columns and sheets. Using various combinations of feeder and dummy tubes over their vertical array of horizontal tubes, the random axial movement of the falling droplets made one dummy tube sufficient to provide a uniform liquid distribution on the lower tubes.

Although the Lorenz and Yung (1978, 1979) correlation presented earlier predicted their data reasonably well, Fujita and Tsutsui (1994) proposed the new more detailed multi-zone model, depicted in Figure 14.12, with a stagnation region, impingement flow region, thermal developing region and a fully developed region. Since the impingement zone is only a small fraction of the tube perimeter, they ignored

it for simplicity. They assumed that the thermal boundary layer grows from the stagnation point at the top of the tube around its perimeter. In the thermally developing zone ($0 < \phi < \phi_d$), the liquid film absorbs the sensible heat conducted into it with negligible evaporation, and this zone ends when the growing thermal boundary layer reaches the liquid film interface. In the fully developed zone ($\phi_d < \phi$), the process is first characterized by simultaneous superheating of the film and partial evaporation of the film at its interface as the temperature profile in the film gradually changes from its 3rd order polynomial profile at the beginning of the zone to a linear profile (i.e. one-dimensional conduction). Then, for all larger angles up to $\phi = \pi$, all the heat conducted into the film from the wall is assumed to evaporate at the film interface. They also proposed an empirical correlation that reasonably predicted their test data.

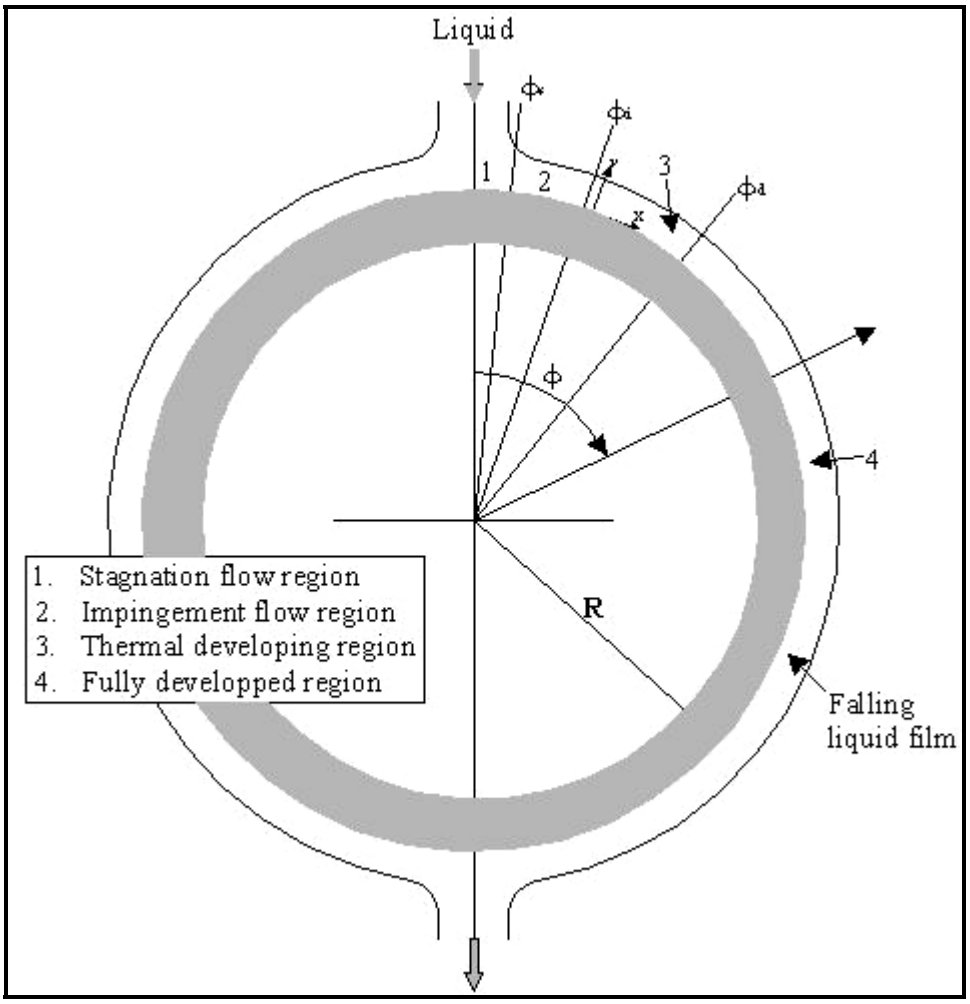


**Figure 14.12. Three zone model of Fujita and Tsutsui (1994).**

In a review on falling film evaporation on vertical surfaces, but also pertinent to horizontal tubes, Gross (1994) discussed the problem of dry patch formation. He concluded that formation of a dry patch was an instability problem, influenced by the following forces on the film:

- ***Liquid inertia forces***. The static pressure head within the liquid film at its stagnation point at the top edge of a dry patch favors rewetting of the dry patch;
- ***Surface tension forces***. The surface tension forces at the interface of the film have a tendency to enlarge the size of a dry patch;

- ***Marangoni effect***. The surface tension gradient created by the temperature profile within the film, particularly near the boundary of a dry patch, acts to transport liquid away from the edge and hence to enlarge the dry patch;
- ***Vapor inertia forces***. The acceleration of the vapor-phase adjacent to the evaporating film acts to increase or decrease the dry patch size depending on the direction of the vapor;
- ***Interfacial shear forces***. These forces create two competing effects on a dry patch size, one trying to spread the liquid and rewet its top edge and the other trying to elongate its lower edge.

However, no method to predict the onset of dry patch formation was provided.

Chen et al. (1994) obtained falling film heat transfer coefficients for tests with R-11 on the outside of two vertical tubes: a plain tube and a Wolverine enhanced pool boiling Turbo-B tube. They did not measure local values but instead mean heat transfer coefficients for their 1.8 m (5.9 ft) long test sections. Figure 14.13 depicts their test data. The falling film performance of the Turbo-B tube was similar to its pool boiling performance. In addition, the enhanced surface was observed to be particularly beneficial in retarding dry patch formation compared to the plain tube (apparently by capillary forces at the pores), thus allowing higher heat fluxes to be reached before complete dryout of the film. Hence, an enhanced boiling tube can potentially achieve a higher maximum vaporization fraction operating under falling film conditions compared to a plain tube, in addition to augmenting heat transfer.

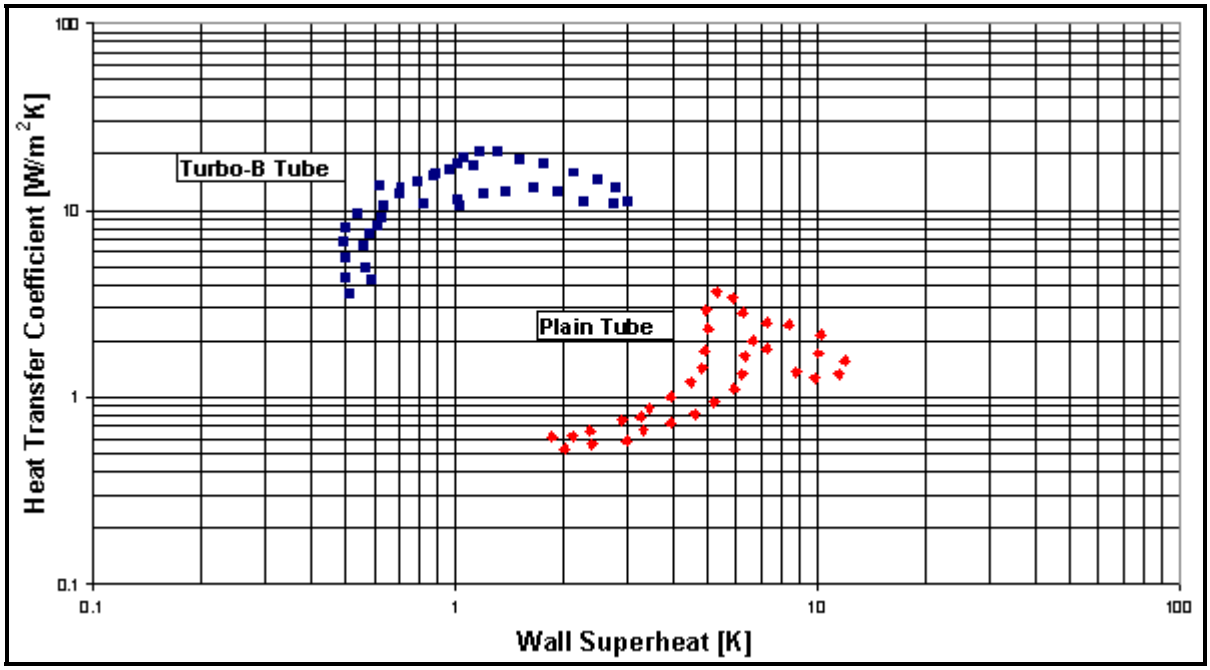


**Figure 14.13. Falling film test results for R-11 of Chen et al. (1994).**

Fluid spray distribution rates and axial flow rate uniformity were studied by Zeng et al. (1994) on horizontal tube bundles to investigate geometry effects on 3 by 1 tube arrays, i.e. 3 tubes wide and only one row deep. All tubes were 19.05 mm in diameter. A plain tube array, a low finned tube array and a grooved tube array were tested. The low fin tubes had 1575 fpm (40 fpi) with fins 0.97 mm high and 0.33 mm thick. The grooved tubes had 60 longitudinal grooves around the perimeter with a 0.64 mm depth and a 0.4 mm pitch. They observed that the plain tube bundles attained more uniform liquid distribution than the low fin bundles because the fins prevented the liquid film from spreading along the axis of the tube; the grooved tube bundle functioned similar to the plain tube bundle. Consequently, significant non-

uniformity in the local flow rates occurred on the low fin tube bundle but quite uniform distribution was achieved for the other tubes.

Moeykens and Pate (1994) measured heat transfer coefficients for falling film evaporation of R-134a at a saturation temperature of 2°C on two different single, plain horizontal tubes. They were copper tubes of 12.7 mm and 19.05 mm diameter, respectively. They investigated the use of a wide-angle, low-pressure-drop (0.02 Mpa, 3 psi) nozzle compared to a high-pressure-drop (0.86 MPa, 125 psi) nozzle, noting the following trends:

- ***Tube diameter effect***: the 12.7 mm tube gave 5-10% better performance than the 19.05 mm tube;
- ***Liquid overfeed effect***: heat transfer was not affected by the refrigerant flow rate, if it was sufficient to avoid dry patch formation, since nucleate boiling dominated at their test conditions;
- ***Nozzle type***: the high-pressure-drop nozzle yielded better heat transfer because of its impinging jet spray on the top of the tube while the low pressure nozzle provided a wider angle of spray;
- ***Relative performance***: the falling film coefficients were higher than the corresponding pool boiling coefficients measured on the same tubes.

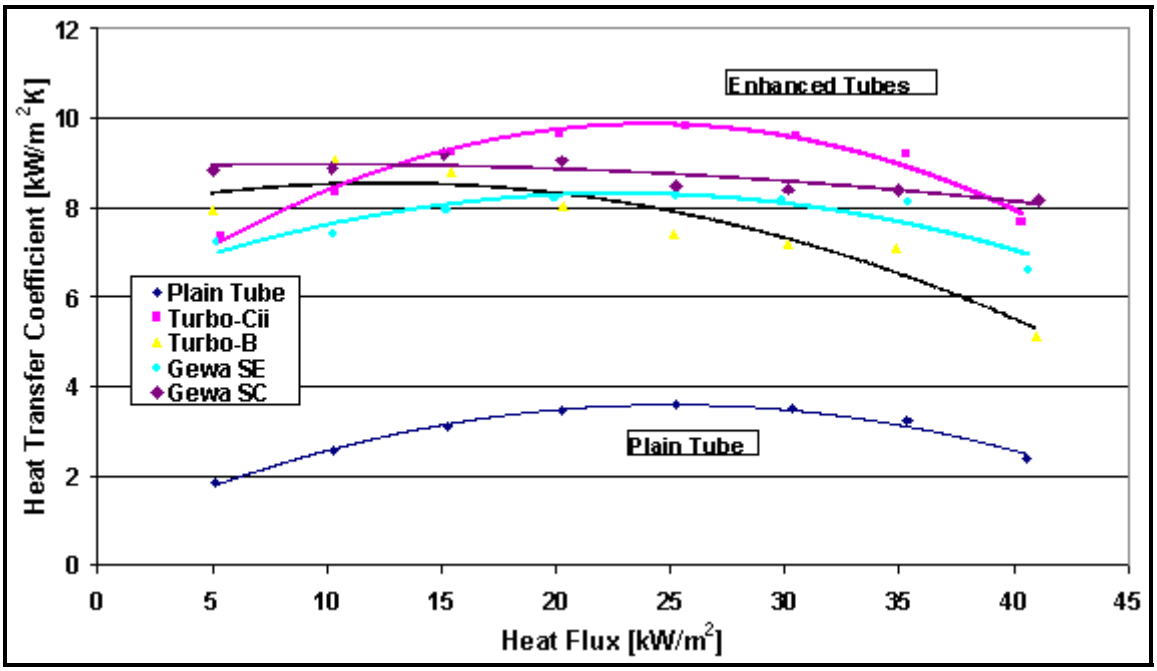


**Figure 14.14. Falling film coefficients for R-134a on single enhanced tubes from Moeykens et al. (1995a).**

Moeykens et al. (1995a) continued the above study, extending it to R-134a and R-134a/oil mixtures in single-tube tests at 2°C and tested four types of tubes: an enhanced pool boiling tube (Turbo-B), three enhanced condensation tubes (Turbo-Cii, Gewa-SC and Gewa-SE), two low fin tubes (1575 fpm/40 fpi, 1024 fpm/26 fpi) plus a plain tube, all about 19 mm in diameter. Note that first types of tubes have three-dimensional types of enhancement geometries while the low fins are considered as two-dimensional enhancements. Figure 14.14 shows a comparison of the 3-d enhanced tubes to the plain tube for pure R-134a, where the enhanced *condensing* tubes outperformed the Turbo-B, almost certainly because they were more effective in promoting the formation of thin liquid films similar to what they were designed to do for falling film *condensation*. The falloff in the heat transfer coefficients at high heat fluxes occurred because of dry patch formation on the tubes. The low fin tubes (not shown in Figure 14.14) gave

performances in the range of about 6000-7500 W/m$^2$K, less than the enhanced geometry tubes. Adding small mass fractions of polyol-ester lubricating oils to R-134a, viscosity grades of 32cs and 68cs, the heat transfer increased when foaming occurred. Overall, the best performing falling film tube was the Wolverine Turbo-Cii.

Moeykens et al. (1995b), in the next phase of their study, tested small tube bundles comprised of 20 tubes. These tests were run with pure R-134a with liquid overfeed ratios from 1.4 to 7.9 at 2°C. The overfeed ratio is defined as $\Gamma_{feed}/\Gamma_{evap}$, where $\Gamma_{feed}$ is the flow rate of liquid applied to the top of the array and $\Gamma_{evap}$ is the flow that has been evaporated when reaching the bottom of the array. Both square and triangular tube layouts were utilized for the same types of tubes as above, with the exception of the 1024 fpm (26 fpi) low fin tube. The refrigerant was sprayed onto the top of the bundle using low pressure drop, wide-angle, solid-cone nozzles. Bubbles were visible in the thick liquid layer at the bottom of the tubes, indicating nucleate boiling was occurring in the films on all the tubes. The enhanced condensation tube Turbo-Cii again gave by far the best performance. In fact, the Turbo-Cii tube bundle operating in the falling film mode nearly doubled the pool boiling performance of the Turbo-B bundle.

Moeykens and Pate (1995) also investigated the influence of nozzle height and orifice size for spray evaporation of R-134a at 2°C on one 1575 fpm (40 fpi) low fin tube bundle with 20 tubes in a triangular tube layout. The vertical tube pitch was 19.1 mm, the horizontal tube pitch was 22.2 mm, and the tube diameter over the fins was 18.70 mm. Five different nozzle orifice diameters from 4.0-5.6 mm were tested in either circular or square spray patterns. The 0.0172 MPa (2.5 psi) pressure drop nozzles were located from 41.3 to 66.7 mm above the top tube row. The falling film coefficients at the optimal film-feed rate were higher than those obtained for pool boiling on the same tube bundle. Regarding the objective of obtaining uniform liquid spray over the top tube row, the advantage of a square nozzle spray pattern compared to a circular spray pattern became insignificant with increasing overlap of the sprays from adjacent nozzles. This small bundle was prone to local dryout on the bottom tube rows because the low fins inhibited longitudinal spreading of the liquid film along the tubes.

Moeykens and Pate (1996) continued these tests, investigating staggered tube bundles with four types of tubes: plain, 1575 fpm (40 fpi) low fin, Wieland Gewa-SC and Wolverine Turbo-B. Oil effects were checked using 340 SUS polyol-ester oil with 1.0 and 2.5 wt.% oil in the liquid feed of R-134a onto the top of the tubes. The tube bundles had the same geometry as their prior low finned tube bundle. R-22 with 300 SUS alkyl benzene oil was also tested on the plain tube and Turbo-B tube bundles. The results for two types of the tubes are compared in Figure 14.15, where the heat transfer coefficient is the mean for the bundle from individual measurements on the central vertical tube row of 4 tubes. These oils promoted foaming, which was thought to retard the formation of dry patches and hence was beneficial for heat transfer at higher heat fluxes. The oil improved plain tube and Turbo-B tube heat transfer but with the benefit decreased for the Turbo-B with increasing heat flux.

Moeykens et al. (1996) next extended their falling film fluid database to R-123 and R-123/oil mixtures for staggered and inline tube bundles. Plain, Turbo-Cii and Turbo-B tubes were tested at a saturation pressure of 0.0357 MPa. A 303 SUS naphthenic mineral oil was used with R-123. Curiously, foaming was only observed on the plain tube bundles. For R-123, the Turbo-B tube provided better performance than the Turbo-Cii and its falling film performance was about 2-2.6 times that of its pool boiling performance in R-123! The oil improved Turbo-Cii performance by up to 90% at some test conditions but degraded it at others, depending on the liquid feed flow rate. High performance was observed without foaming on the enhanced tubes and, consequently, it may be that foaming does not increase resistance to dry patch formation as suggested in their earlier study.

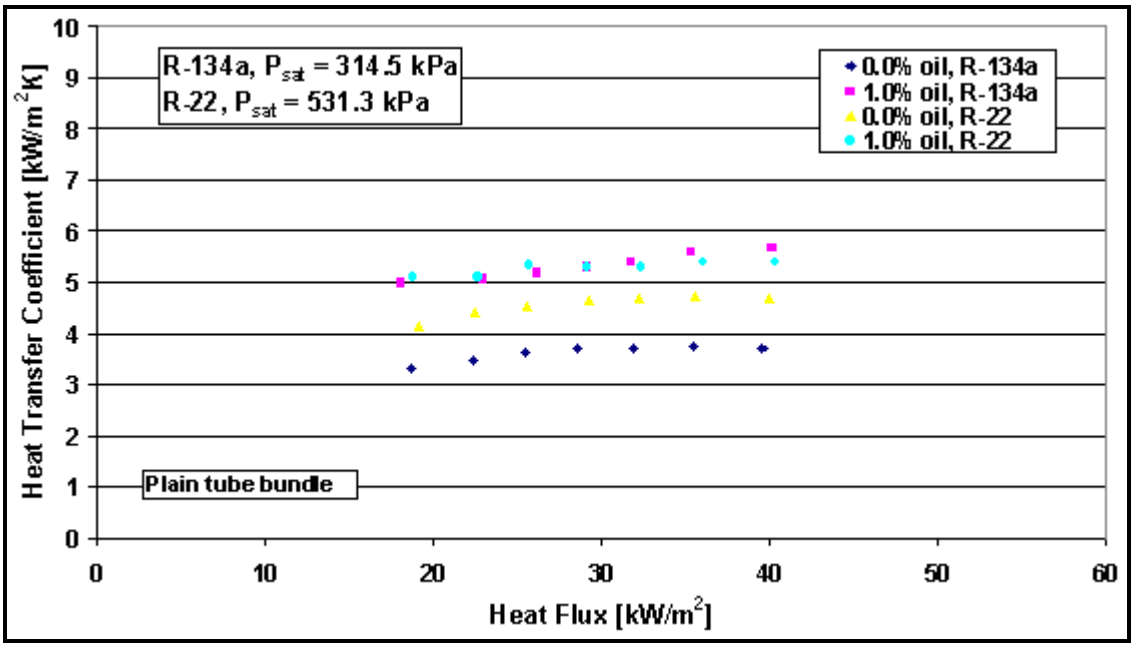


(a)

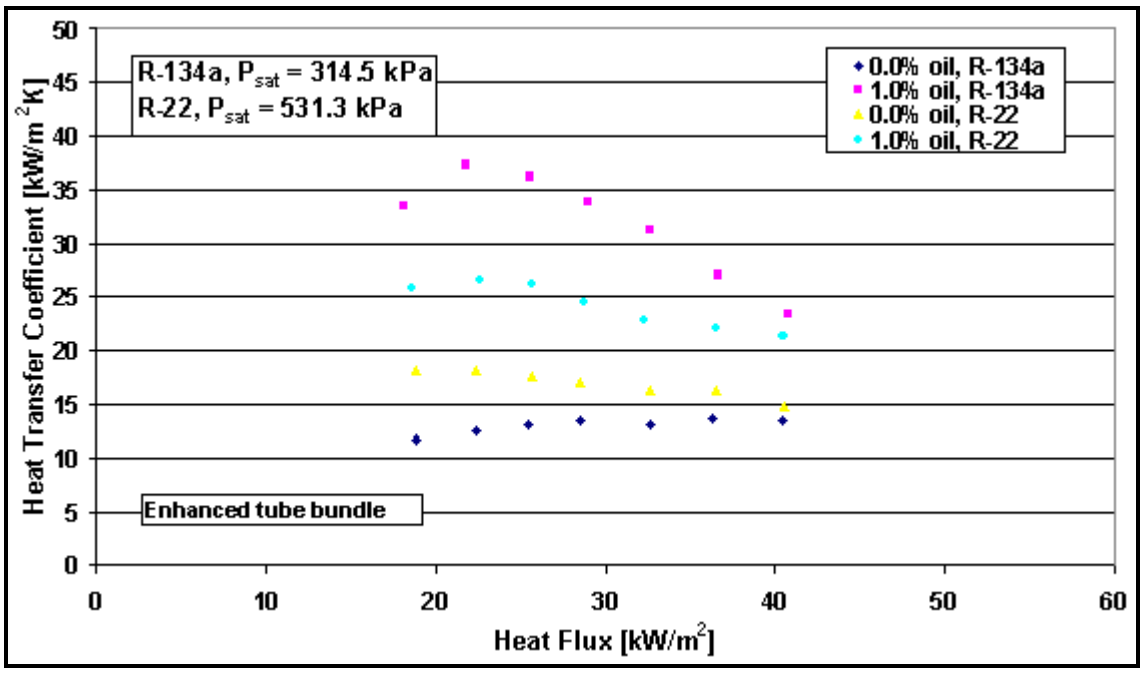


(b)

**Figure 14.15. R-22 and R-134a tests with and without oil on triangular pitch tube bundles of Moeykens and Pate (1996): (a) plain tube, (b) Turbo-B tube.**

Regarding other effects of oil on the falling film evaporation process, oil may have an effect on the falling film modes from tube to tube due to the higher surface tension and viscosity of the oil, e.g. this may convert the intertube film flow from column mode to sheet mode. Another mechanism that may well be important is liquid retention (in a further analogy between enhanced falling film evaporation and condensation), which may be the reason that the Turbo-B outperformed the Turbo-Cii for R-123 while the opposite was observed for R-134a. The Turbo-Cii, being an enhanced condensation surface, retains

liquid between adjacent fins on the lower portion of the tube; hence minimizing the liquid retention angle and the film thickness are important, both values which would tend to increase in value with the larger surface tension of R-123 compared to R-134a. On the contrary, the Turbo-B tube promotes thin film evaporation inside its reentrant channels and is thus much less susceptible to liquid retention since its pore openings act as self-regulating orifices for controlling the liquid flow rate into the reentrant channels.

The mass transfer resistance created by the oil in evaporation of the liquid film is detrimental to heat transfer, having a larger influence on the Turbo-B tube (like in pool boiling) since it has the higher pure fluid performance. Since the oil is non-volatile, its tends to build up its concentration at the evaporating interface, which in turn increases the local bubble point temperature of the refrigerant-oil mixture at the interface. For nucleate pool boiling, this effect has been explained in Thome (1996) for refrigerant-oil mixtures with the expression

$$\frac{\alpha}{\alpha_I} = \frac{(T_w - T_{bub})}{(T_w - T_{bub}) + dT_{bub}} \qquad [14.6.1]$$

where $\alpha$ is the actual heat transfer coefficient, $\alpha_I$ is the ideal coefficient of the pure refrigerant, $(T_w - T_{bub})$ is the wall superheat for the pure refrigerant without oil at the specified heat flux, and $dT_{bub}$ is the rise in the bubble point temperature from its bulk value to the interfacial value at the vapor-liquid interface as a result of the depletion of refrigerant in the liquid boundary layer adjacent to the interface where the oil cannot evaporate. The effect is to reduce the superheat available for the evaporation process. This mass transfer resistance effect increases with heat flux, from no effect at zero heat flux up to a significant impact at high heat flux where the evaporation rate of the refrigerant reaches its highest level and thus increases $dT_{bub}$ across the diffusion boundary layer. Consequently, the mass transfer effect tends to decrease the ratio $(\alpha/\alpha_I)$ with increasing heat flux while on the other hand the oil may impact on the value of $\alpha_I$ by a direct influence on the heat transfer mechanisms themselves.

Hu and Jacobi (1996a) investigated adiabatic falling film modes on vertical tube rows, i.e. droplet, column, sheet and their combinations, in an experimental program with four plain tubes in a vertical tube row, where the top tube acted as the liquid distributor. The fluid from the feed tube flowed over the second tube and then onto the third tube which acted as the test tube, and then onto the bottom 'dummy' tube, and finally into an open liquid catching tube. Air flow from top to bottom was applied at velocities up to 15 m/s by placing the test set up in a wind tunnel. Water, ethylene glycol, water/glycol, oil and alcohol were tested. The flow patterns and heat were categorized into droplet, droplet-jet, in-line jet, staggered jet, jet-sheet and sheet modes, where some are transition modes from one regime to another. Empirical correlations for the transition boundaries were determined (presented earlier in this chapter). In Part 2 of their study, Hu and Jacobi (1996b) measured falling film heat transfer coefficients to subcooled liquid (without evaporation) for test conditions similar to the above tests. They presented empirical correlations for predicting heat transfer coefficients for film Reynolds numbers up to about 1900 for a wide range of fluid properties, including the ratio of vertical intertube spacing (S-D) to tube diameter D. The following expressions were proposed:

Sheet mode: $$Nu_{\Gamma,sub} = 2.194\, Re_{\Gamma}^{0.28}\, Pr_L^{0.14}\, Ar_L^{-0.20} \left(\frac{S-D}{D}\right)^{0.07} \qquad [14.6.2]$$

Column mode: $$Nu_{\Gamma,sub} = 1.378\, Re_{\Gamma}^{0.42}\, Pr_L^{0.26}\, Ar_L^{-0.23} \left(\frac{S-D}{D}\right)^{0.08} \qquad [14.6.3]$$

$$\text{Droplet mode:}\quad Nu_{\Gamma,sub} = 0.113\,Re_{\Gamma}^{0.85}\,Pr_{L}^{0.85}\,Ar_{L}^{-0.27}\left(\frac{S-D}{D}\right)^{0.04} \qquad [14.6.4]$$

The Archimedes number $Ar_L$, based on tube diameter, is defined as:

$$Ar_L = \frac{D^3 g}{\nu_L^2} \qquad [14.6.5]$$

The Nusselt number $Nu_{\Gamma,sub}$ is the same as that defined in Equation [14.5.9] and the film Reynolds number is the same as that defined in Equations [14.4.6] and [14.5.6] based on the liquid flow rate on one side of the tube.

Falling film coefficients for ammonia were measured by Zeng et al. (1995) using commercial spray nozzles for distribution of the liquid overfeed. They tested a single, horizontal plain, stainless steel tube of 19.1 mm diameter at saturation temperatures from -23.3°C to 10°C. Their results are shown in Figure 14.16 compared to a correlation of Parken et al. (1990). In another study, Chyu et al. (1995) did a geometrical analysis on nozzle layouts. Figure 14.17 shows their comparison of the same type of nozzles arranged in a triangular array compared to a square array. There is less overlap of the spray areas using the triangular layout and hence a more uniform liquid distribution is achieved.

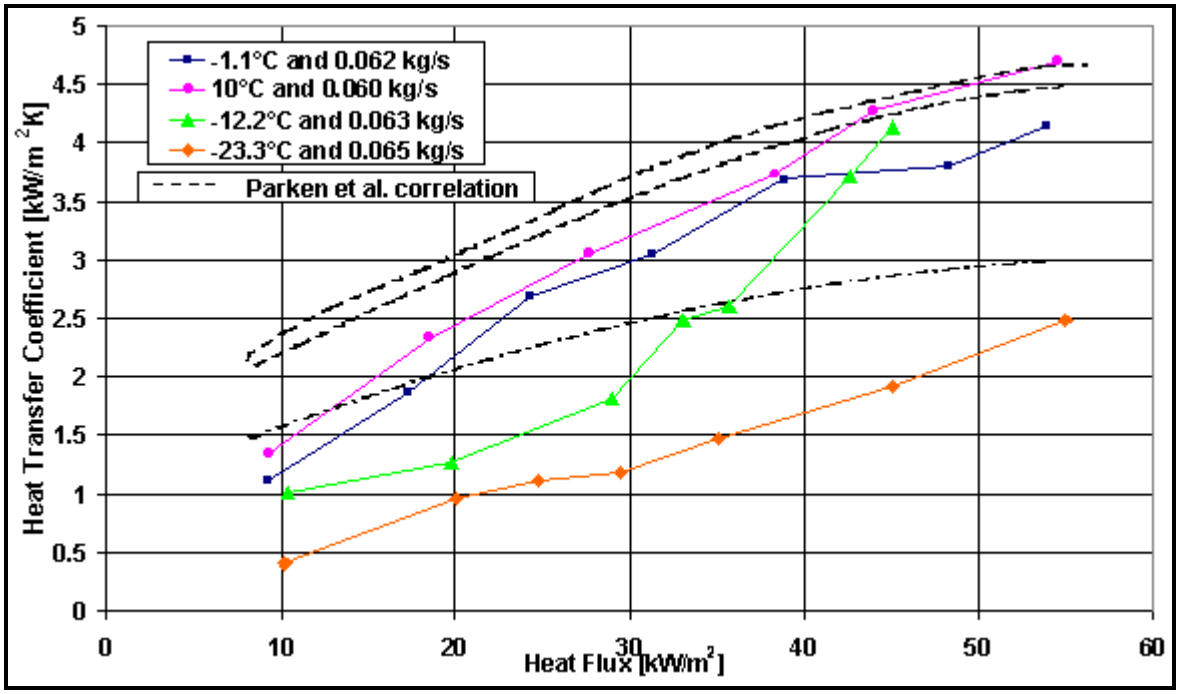


**Figure 14.16. Ammonia falling film results on a single, plain tube from Zeng et al. (1995).**

Zeng et al. (1997) extended their earlier single-tube tests for pure ammonia to a 3-tube by 3-tube square layout with a 1.25 pitch ratio for a horizontal plain tube bundle made with 19.1 mm stainless steel tubes. Saturation temperatures ranged from -23°C to 10°C. They also boiled ammonia on the same small tube bundle to get some bundle boiling performance data as a comparison to falling film performance. Their bundle in the flooded evaporator mode performed only slightly better than predicted for a single tube since the bundle is small with little convection effect, while in falling film mode the performance was

better by a factor of 1.5 to 2 times. These test data covered the range where the influences of both evaporation and nucleate boiling were significant.

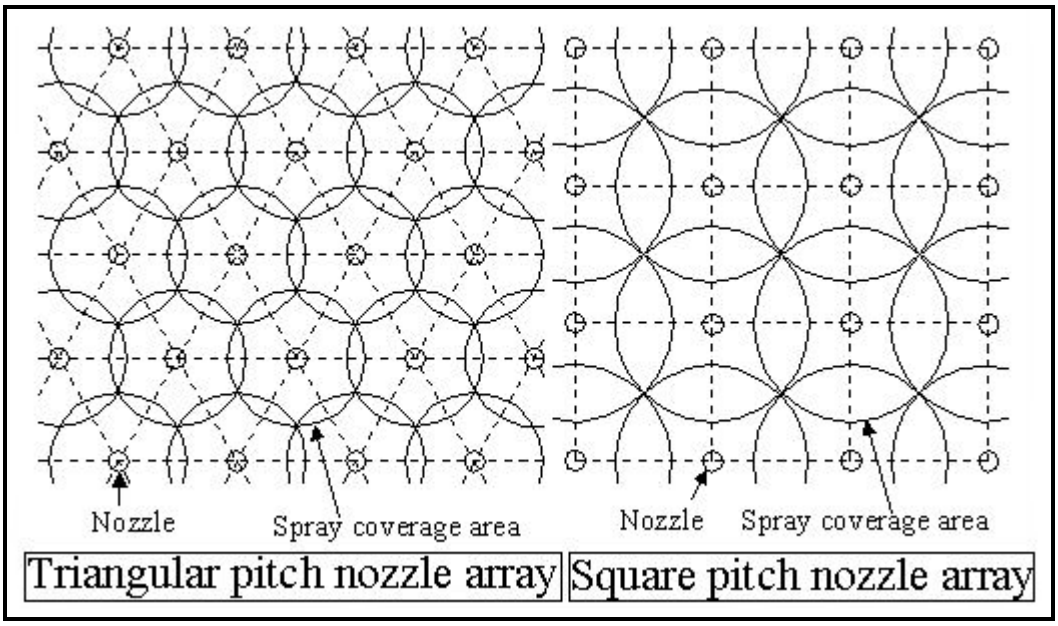


**Figure 14.17. Nozzle spray area layouts. (left) triangular pitch nozzle array, (right) square pitch nozzle array of Chyu et al. (1995).**

Zeng et al. (1998) extended their single-tube tests to falling film evaporation of ammonia to a carbon steel low fin tube and a corrugated tube. Their 1575 fpm (40fpi) low finned tube had a fin tip diameter of 19.85 mm and fin height of 1.0 mm but its surface area per unit length was not cited. The Wolverine corrugated tube was 19.05 mm in outside diameter over the corrugations with a corrugation pitch of 7.94 mm, but the corrugation depth was not cited. A large number of single-tube tests were run at the previously tested saturation temperatures from -23.3°C to 10°C. The low fin tube increased performance by up to 2.8 times with respect to their prior plain tube tests at high heat fluxes where nucleate boiling occurred in the film but offered little augmentation at low heat fluxes. The corrugated tube performed similar to that of the plain tube, i.e. minimal augmentation.

## 14.7 RECENT STUDIES SINCE 2004

Extensive experimental tests on pool boiling and falling film evaporation on plain and enhanced tubes have been undertaken by Thome and co-workers over the past years. The tests have primarily used R-134a as the test fluid but more recently also the refrigerant R-236fa has been added to diversify the fluid properties in their database. The experimental program included testing of plain tubes and enhanced boiling tubes in nucleate pool boiling mode, falling film mode on a single-tube row with up to 10 horizontal tubes one above one another and falling film mode on a three-row bundle with up to 30 tubes in the bundle. This experimental work was then the starting point for improving prediction methods for falling film evaporation. This work is summarized below, with special attention on the plain tube and Wolverine enhanced tube results.

Figure 14.18 depicts some falling film test results for a single-row of 10 horizontal plain tubes placed one over the other with a tube pitch of 22.3 mm with tube diameter of 18.91 mm (odd tube data only here). The outside nominal heat flux is 35.6 kW/m$^2$. Using hot water heating with five tube passes for ten tubes,

the hot water enters the even tube rows, turns around and the passes through the odd tube rows. This configuration creates a nearly uniform evaporation rate after each pair of tubes, such that the falling liquid film remains uniformly distributed along the tube array (*note*: using a one-pass design would create a high heat flux at one end and a low heat flux at the other of the array, creating a very non-uniform liquid distribution down the tube row and initiation of early dryout at the high heat flux end, while instead their setup avoids this pitfall). Thus, any effect of any maldistribution is smallest at the midpoint of their 0.5 m long tubes, and that is where the local heat transfer coefficients of all the tubes were measured. Quite noticeable in their data, there are two distinct trends:

- There is a more or less horizontal plateau in the data for all the tubes at a film Reynolds number greater than 500. The scatter in the data within the plateau is due first to the experimental errors in their measurements and secondly to the range of heat fluxes of about ±10% from the nominal value cited. The plateau is at a much higher heat transfer performance than pool boiling heat transfer measured at the same heat flux on one of the plain tubes (up to about 80%), indicating a substantial enhancement effect of the falling film on the nucleate boiling process in the film.
- The falloff in the heat transfer coefficient at film Reynolds less than 500 was observed visually to be due to the formation of dry patches on the tubes. As the size and residence time of the dry patches increased, the time-averaged local heat transfer coefficient decreased towards an all dry state. Thus, the onset of dryout is an important operating criterion to divide the all wet from the partially-wet operating conditions and thermal performance.

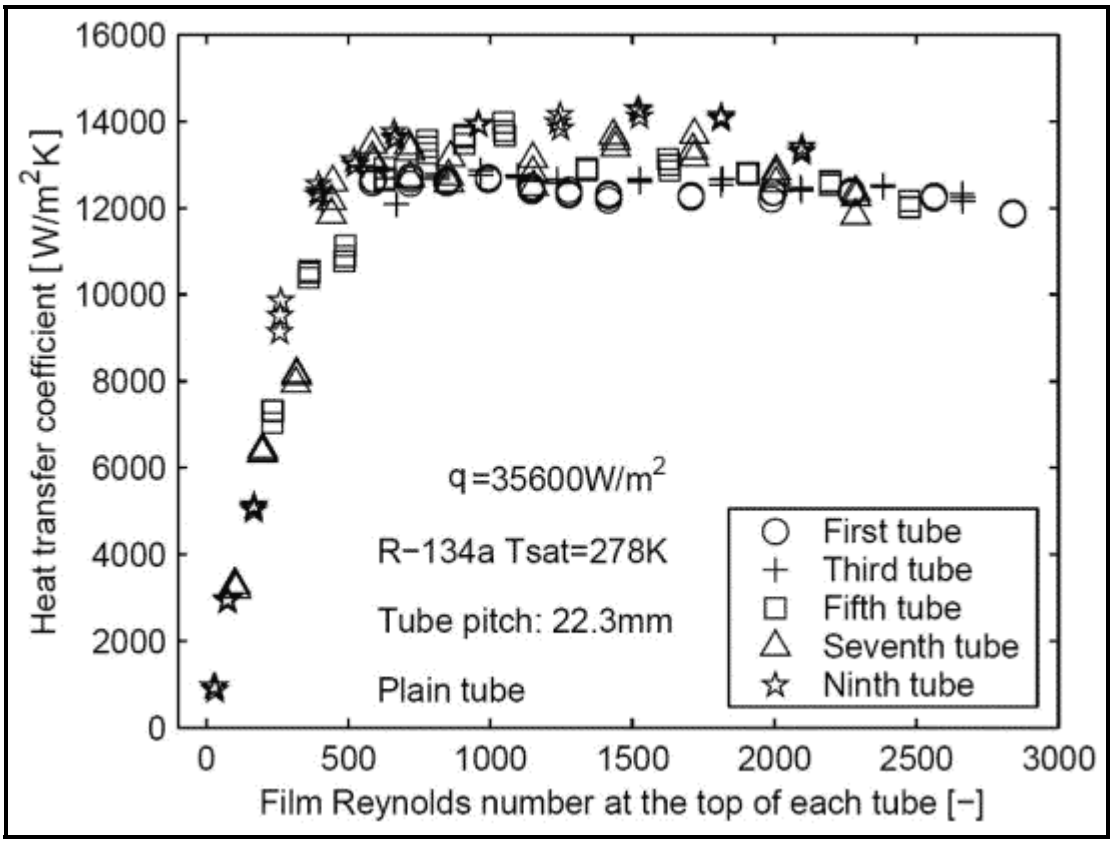


**Figure 14.18. Falling film on a single-row of ten plain tubes from Roques and Thome (2007a) showing odd tube results.**

Figure 14.19 depicts some falling film test results for a single-row of 10 horizontal, Wolverine Turbo-BII tubes placed one over the other with a tube pitch of 22.3 mm with tube diameter of 18.84 mm (odd row tubes only here). The nominal heat flux is 37.2 kW/m$^2$. The same setup for the heating water was also used here. Again, there is a plateau in the heat transfer coefficients above a film Reynolds number of about 500 and a falloff below where the formation of dry patches becomes more extensive. Hence, the optimal design conditions are to maintain the film Reynolds number at the top of each tube above 500 to insure high thermal performance while the tubes below this threshold can instead be immersed in a liquid pool in an actual falling film evaporator to function like flooded evaporator tubes. Notably, the tubes above this threshold will have a nearly uniform thermal performance and hence create a nearly uniform overall heat transfer coefficient. The heat transfer coefficients on the Turbo-BII array in the all wet plateau are a little more than twice those of the plain tube array. Furthermore, the Turbo-BII falling film heat transfer coefficients tended to be on average about 10-15% higher that their corresponding pool boiling values.

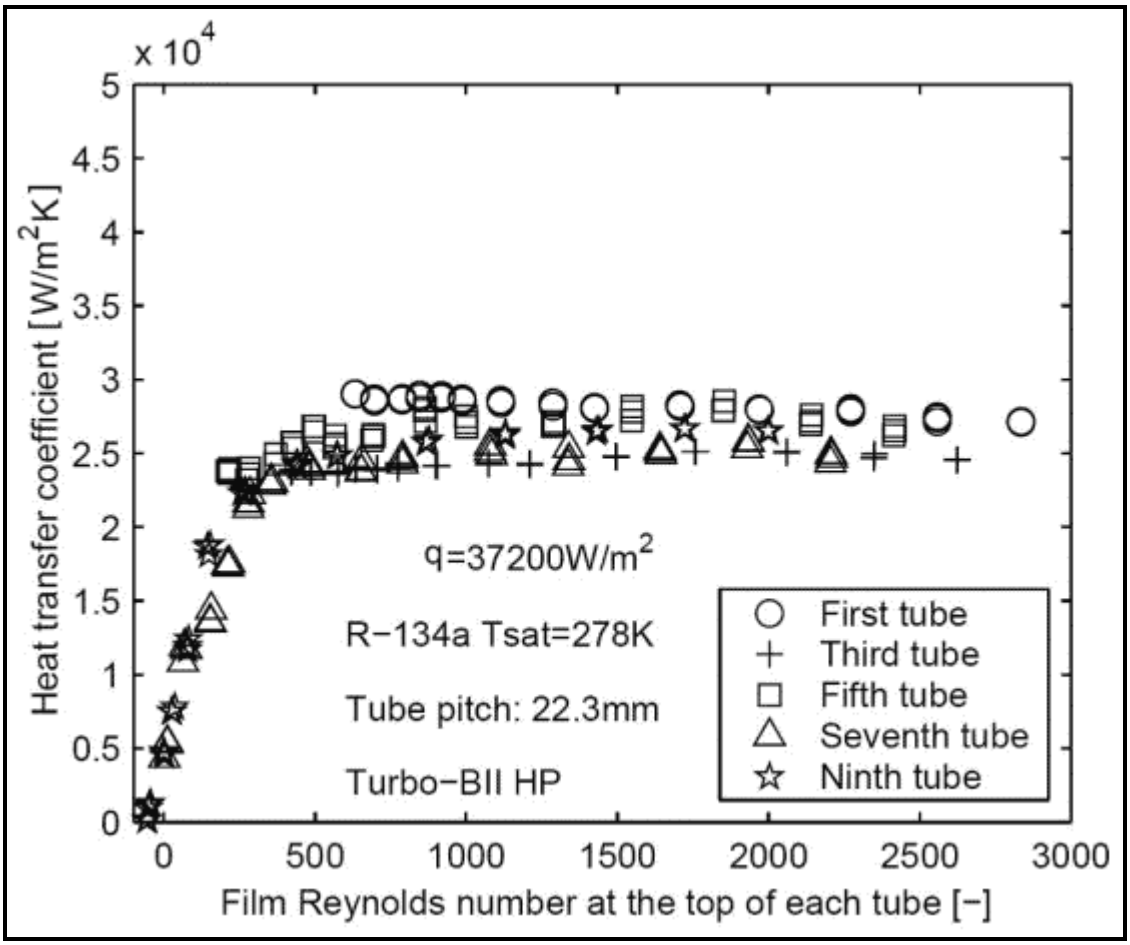


**Figure 14.19. Falling film on a single-row of ten Wolverine Turbo-BII tubes from Roques and Thome (2007a) showing odd row results.**

Figure 14.20 depicts some falling film test results for a single-row of 10 horizontal, UOP High Flux tubes placed one over the other with a tube pitch of 25.5 mm with tube diameter of 18.87 mm (odd tube row data only here). The nominal heat flux is 49.7 kW/m$^2$. The same setup for the heating water was also used here. Again, there is a plateau in the heat transfer coefficients above a film Reynolds number of about 500-600 and a falloff below where the formation of dry patches becomes more extensive. The larger

dispersion of the data in the plateau is primarily due to the propagation of errors in these measurements, which are larger due to the very high heat transfer coefficients from 45000 to 67000 W/m$^2$K. The High Flux falling film heat transfer coefficients tended to be on average about the same as their corresponding pool boiling values.

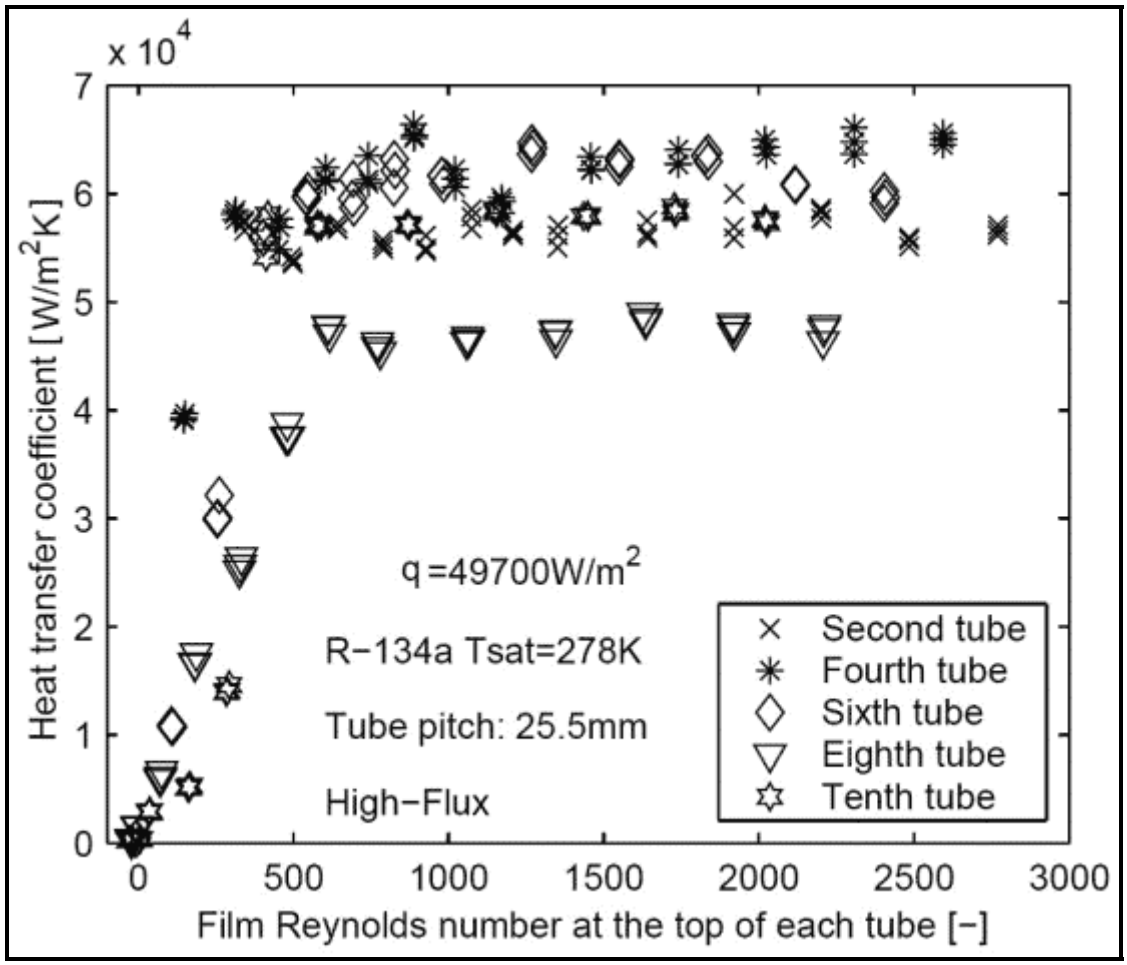


**Figure 14.20. Falling film on a single-row of ten High Flux tubes from Roques and Thome (2007a) showing even row results.**

It is thus interesting to see that the general trend in the data, a plateau of heat transfer coefficients insensitive to the film Reynolds number above the dryout threshold and a rather linear falloff below the threshold, holds for a plain tube, a mechanically enhanced surface tube and a porous coated enhanced tube. Similar data were obtained at other test conditions and also for another enhanced boiling tube. These can be found in Roques and Thome (2007a) and even more details in the thesis of Roques (2004) available for free online.

The more recent results of Habert and Thome (2010a, 2010b) for the new Turbo-EDE2 enhanced boiling tube of Wolverine are shown in Figure 14.21. On the left, results for R-134a are depicted at three nominal heat fluxes, notably with the highest performance at the lowest heat flux where local heat transfer coefficients in the "plateau" averaged about 78000 W/m$^2$K! The mechanism responsible for reducing the performance at higher heat fluxes (but still with heat transfer coefficients from 38000 to 50000 W/m$^2$K) was not identified. Results for a second fluid, R-236fa, gave similar trends but lower performance as this tube was optimized for use with R-134a but not with R-236fa. Once again, the general trends were the

same as those in the earlier tests described above. More details on these tests can be found in Habert (2009).

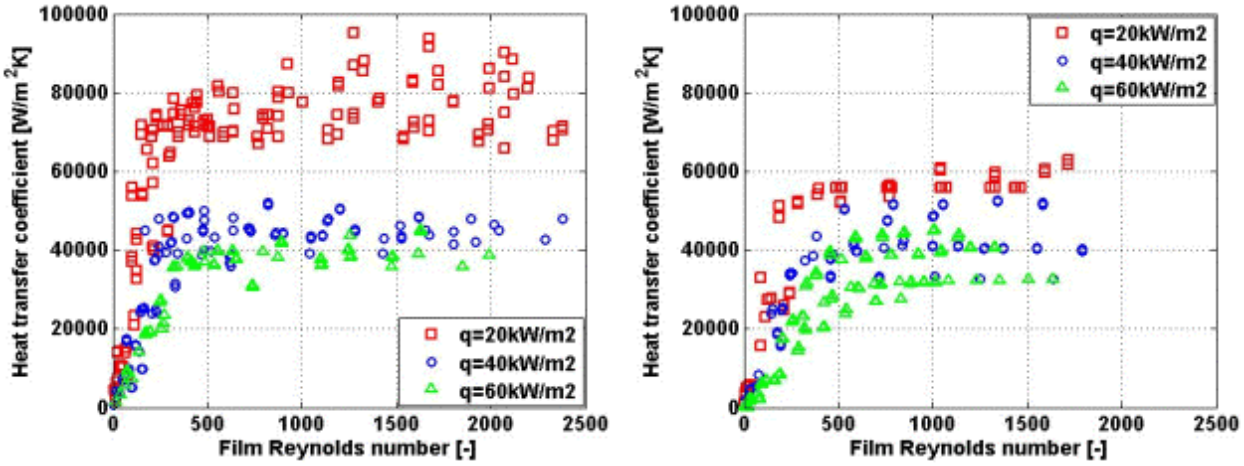


**Figure 14.21. Falling film results on a single-row of ten Wolverine Turbo-EDE2 tubes from Habert and Thome (2010a) for R-134a (left) and R-236fa (right) at 5°C saturation temperature.**

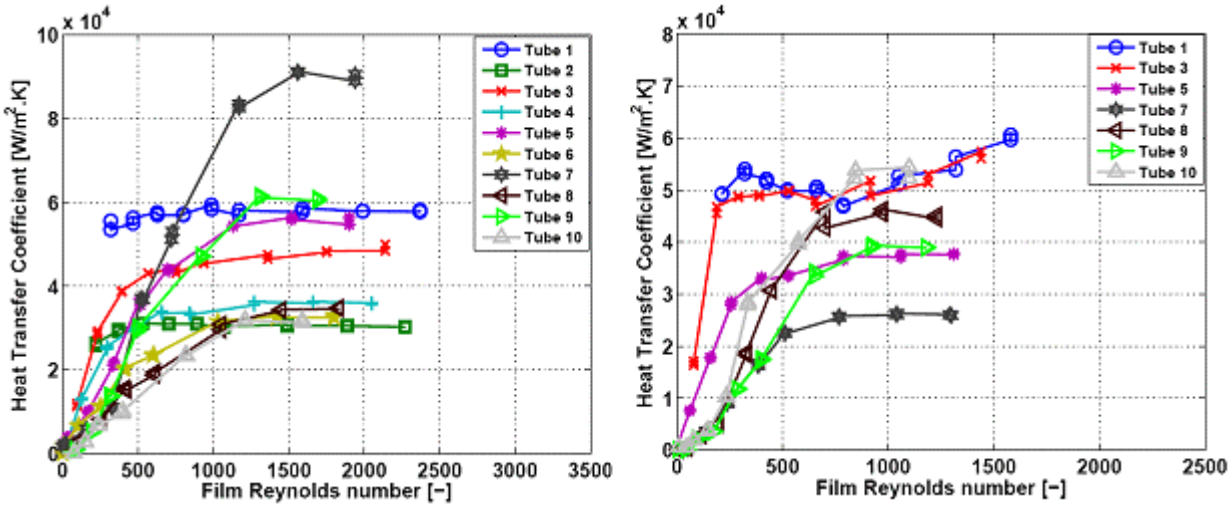


**Figure 14.22. Falling film results on a single-row of ten Wolverine Turbo-EDE2 tubes from Habert and Thome (2010a) for R-134a (left) and R-236fa (right) at 5°C saturation temperature and heat flux of 40 kW/m$^2$.**

Figure 14.22 depicts some bundle falling film heat transfer coefficients that were measured for a 30-tube bundle of Wolverine Turbo-EDE2 tubes that were 0.5 meters long. The same procedure as described above was used to determine the local heat transfer coefficients at the midpoint of each tube in the central row of three rows. The tubes had a 22.30 mm vertical pitch and a 22.30 mm horizontal pitch in a staggered arrangement. Referring to the single-row tests results presented above, the bundle results are approximately in the same range, but exhibit a bundle effect that can increase or decrease the local heat transfer performance. While the bundle results still illustrate a plateau and a drop off in performance at lower film Reynolds numbers, the distinction is now less clear. The reason for this is believed to be due to the non-ideal liquid distribution within the bundle (all tubes were wetted and in nucleate boiling conditions). The liquid may preferentially flow around one side of a tube and not the other side; for

instance, creating a local partially wet condition due to flow maldistribution rather than dry patch formation. Thus, a lower tube may have a higher heat transfer coefficient than the tube above it.

For the prediction of falling film heat transfer coefficients (all data with nucleate boiling present in the film), Roques (2004) and Roques and Thome (2007b) proposed a simple correlation for plain and enhanced tubes to predict the falling film heat transfer coefficient on a single-row (array with up to 10 tubes) when the tubes are all wet (no dryout patches):

$$\alpha_{array} = \alpha_{wet} = \alpha_{nb} K_{ff} \qquad [14.7.1]$$

Their multiplier $K_{ff}$ represents the effect of falling film on the nucleate pool boiling heat transfer coefficient on the same tube at the same operating conditions. Based on their R-134a data, $K_{ff}$ was correlated as a function of the tube pitch and heat flux as:

$$K_{ff} = \left(1 + b_1 \frac{L_{pn}}{L_{pn,ref}}\right)\left(b_2 + b_3\left(\frac{q}{q_{DNB}}\right) + b_4\left(\frac{q}{q_{DNB}}\right)^2\right) \qquad [14.7.2]$$

The heat flux q is for the particular tube in the array, giving the heat transfer coefficient for that tube, with $\alpha_{nb}$ evaluated at this value of q. In this empirically fit equation, the tube pitch normal to direction of flow $L_{pn}$ (i.e. the vertical tube pitch) is non-dimensionalized with the minimum tube pitch tested, $L_{pn,ref}$ = 22.25 mm, and the heat flux q is non-dimensionalized using the departure from nucleate boiling heat flux $q_{DNB}$ from Kutateladze's correlation (1948) that was discussed in Chapter 9:

$$q_{DNB} = 0.131\, \rho_G^{1/2}\, h_{LG} \sqrt[4]{g(\rho_L - \rho_G)\sigma} \qquad [14.7.3]$$

The method takes the nucleate pool boiling curve of the tube/fluid combination as an input. It can be calculated for a plain tube (see methods in Chapter 9) or taken from an experimental pool boiling curve, which is a necessity for enhanced boiling tubes since no general method is available to predict them. The tube pitches center-to-center in the vertical tube array of horizontal tubes tested were: 22.25 mm, 23.9 mm and 25.5 mm (which represent vertical spacing between the tubes of about 3.4, 5.0 and 6.6 mm in respect to the nominal outside tube diameters. They performed their experiments within a heat flux range from about 20 to 60 kW/m$^2$ and extrapolating to lower heat fluxes that might be typical of actual design is not advised. For R-134a at 5°C in particular, $q_{DNB}$ is 361.3 kW/m$^2$.

**Table 14.2. Empirical constants for the falling film coefficient prediction.**

| Tube: | Plain Tube | Turbo-BII HP | High Flux |
|---|---|---|---|
| $b_1$ | -0.335 | -0.361 | -0.0104 |
| $b_2$ | 2.059 | 2.891 | 0.540 |
| $b_3$ | 2.370 | -16.314 | 5.723 |
| $b_4$ | -7.793 | 59.906 | -4.714 |

The values of the empirical constants are given in Table 14.2 for some of the tubes they tested. The constant $b_1$ accounts for the tube pitch influence and its value is nearly the same for the plain and Turbo-BII HP tubes. This value is negative, indicating that the value of the falling film coefficient decreases as the tube pitch increases. The decrease in heat transfer is approximately 8% from the smallest to the largest

pitch, indicating that the velocity of the liquid impinging on the top of each tube has a negative impact on heat transfer, perhaps by having an adverse effect locally on the nucleate boiling process; however, the 8% found here is only a minor impact. For the High Flux tube of UOP, this influence is only 1% from the minimum tube pitch to the maximum one and hence negligible. In actual falling film evaporators, the tube pitch will normally be close to the smallest pitch they tested.

The heat flux has a weak influence on the falling film factor $K_{ff}$ of the plain tube, which has a mean value of 1.4. This means that the performance in falling film evaporation conditions is thus on average 40% higher than in pool boiling. Zeng, Chyu and Ayub (1996) for their bundle with ammonia found a falling film enhancement of about 1.5 to 2 for a plain tube while Danilova, Burkin and Dyundin (1976) found respectively values of 1.5, 1.4 and 1.33 for R-22 at a heat flux of 16 kW/m$^2$ and saturation temperatures of 273, 253 and 233 K. For the Turbo-BII HP, the falling film factor ranged from 1.3 at 20 kW/m$^2$ to 1.15 at 50 kW/m$^2$. For the High Flux tube, the falling film factor increased nearly linearly with the heat flux from 1.0 to 1.5, which is the opposite of its nucleate pool boiling heat transfer coefficient that decreased by a factor of 1.4 in this heat flux range. The falling film heat transfer coefficient of the High Flux tube consequently only increased slightly with heat flux.

More recently, Ribatski and Thome (2007) developed a predictive method for plain tubes with R-134a to characterize both the *all wet* and *partially-wet* conditions. They defined an objective criterion to characterize the onset of dryout based on $K_{ff}$. The onset of dryout (i.e. formation of dry patches) was defined by a drastic decrease of the heat transfer coefficient with decreasing film flow rate and a decrease in the average heat flux. This criterion was used to segregate the experimental data as either being under all wet or partially-wet conditions. In their method, for partial wetting of the tube caused by the dry patches, the heat transfer area was divided into all wet and all dry regions respectively governed by nucleate boiling heat transfer and natural convection heat transfer to the vapor. The local external heat flux and heat transfer coefficient were determined by:

$$\begin{cases} q = q_{wet} F + q_{dry}(1-F) \\ \alpha_{array} = \alpha_{wet} F + \alpha_{dry}(1-F) \end{cases} \qquad [14.7.4]$$

In these expressions F represents the apparent wet area fraction defined as the ratio between the wet area and the total area of the tube's nominal outside surface. Based on a regression analysis of the all wet data in the plateau, a simple correlation of $\alpha_{wet}$ was obtained, following a Cooper-type expression for pool boiling:

$$\alpha_{wet} = 376\, p_r^{0.22} q_{wet}^{0.38} \qquad [14.7.5]$$

The values of $\alpha_{dry}$ were calculated using a correlation for free convection assuming a quiescent vapor condition within the falling film evaporator. Notably, the $\alpha_{dry}$ is much smaller than $\alpha_{wet}$ so its value can be neglected for all practical purposes. Using the partially-wet database and the above expressions, values of F were backed out and correlated as function of the film Reynolds number:

$$F = a\, Re_{top}^{b} \qquad [14.7.6]$$

The empirical values are: a = 0.0024 and b = 0.91. Their prediction method captured the heat flux effect on the heat transfer coefficient and the onset of dryout.

Habert and Thome (2010a, 2010b) and Habert (2009) analyzed their new data and the previous data of Roques (2004) to formulate an improved method for predicting the onset of dryout (to divide the all wet regime from the partially-wet regime) and an updated method for predicting the heat transfer coefficients in each regime. To begin with, the falling film evaporation prediction process is composed of five steps:

1. Prediction of the *film Reynolds number at onset of dryout* to define the transition between all-wet and partially-wet tube surface operation;
2. Prediction (or measurement) of the nucleate pool boiling curve to obtain the *nucleate pool heat transfer coefficient* for the particular tube/fluid combination at the design saturation temperature;
3. Prediction of the *local heat transfer coefficient for the all-wet region on a single-row* with respect to the nucleate pool boiling performance;
4. Prediction of the *local heat transfer coefficient for the partially-wet region on a single-row*, characterized by a rapid decrease of the heat transfer coefficient with increasing dry area fraction;
5. Prediction of the *local bundle heat transfer coefficient* by accounting for the bundle effect with respect to the single-row performance.

Their method focuses primarily on the all-wet data as they are the most important for actual falling film evaporator applications since partially-wet operation will have quite poor thermal performance. Inclusion of the partially-wet design method is primarily important such that one can simulate a bundle's performance also at "off-design" operating conditions.

**Prediction of Film Reynolds Number at Onset of Dryout**. Based on the results from Habert (2009) and the previous results of Roques (2004), the characteristic film Reynolds numbers for onset of dryout were found to be primarily a function of heat flux for the two fluids tested (R134a and R-236fa) for plain and enhanced tubes. The onset of film breakdown Reynolds number increased with increasing heat flux for all tested surfaces, following a similar trend for both fluids. A single form of prediction was thus used for these tube/fluid combinations. The parameters that significantly vary between the two fluids and that could affect the onset of dryout are the local heat flux q, the dynamic liquid viscosity $\mu_L$, the latent heat of vaporization $h_{LG}$ and the tube diameter D. A parameter analysis in Habert and Thome (2010b) leaded to the following dimensionless expression for the film Reynolds number at the onset of dryout at the top of the tube:

$$\mathrm{Re}_{onset} = 65.8\left(\frac{q\,D}{\mu_L h_{LG}}\right)^{0.63} \qquad [14.7.7]$$

This new expression proposed for the onset of film breakdown takes into account fluid properties and heat flux effects and gives a good agreement based on a large database. For the plain and enhanced tubes tested by Habert (2009) and the previous study of Roques (2004), the expression was found to predict 81.6% of the data within ±30% for the 10 tube/fluid combinations out of 11 total (including the plain tube, the High Flux tube, the Turbo-BII HP tube and the Turbo-EDE2 tube) under single-tube row conditions. Extrapolating this expression to tube bundles, the location of the onset of dryout in a tube bundle can be determined from a row by row energy balance starting at the top of the bundle. Thus, the rate of overfeed required to avoid the onset of dryout can be calculated or the number of tubes adjusted.

**Prediction of Heat Transfer on a Single-Tube Row for All-Wet Condition**. The heat transfer method proposed by Habert and Thome (2010b) is an updated combination of the methods of Roques and Thome (2007b) and Ribatski and Thome [11]. Their new method gives good agreement when applied to the new database of Habert and Thome (2010a) and the previous database of Roques (2004) applying the appropriate empirical constants. Their new method obtained a good prediction of the local heat transfer

coefficient for all wet conditions with the pool boiling correlation (or boiling curve fit to the experimental pool boiling data) for each given tube/fluid combination, using two empirical constants to obtain the falling film multiplier $K_{ff}$:

$$\alpha_{array} = \alpha_{wet} = K_{ff}\,\alpha_{nb} \qquad [14.7.8]$$

$$K_{ff} = c\left(\frac{q}{q_{DNB}}\right)^{d} \qquad [14.7.9]$$

The value of $\alpha_{nb}$ is determined at the heat flux q on the particular tube in the array and $q_{DNB}$ is determined using Kutateladze's correlation (1948) described earlier. The values of c and d for a selection of tubes they tested are given in Table 14.3. It was not possible to collapse all the data onto just one set of constants c and d to reflect how the particular surface interacts with the falling bubbly film. The method is applicable to a range of heat fluxes from about 20 to 60 kW/m$^2$ and does not necessary extrapolate well at all to lower heat fluxes. The method is also applicable up to film Reynolds numbers of about 2500.

**Table 14.3. Coefficients for $K_{ff}$ for the new database.**

| | R-134a | | R-236fa | |
|---|---|---|---|---|
| **Tube** | **c** | **d** | **c** | **d** |
| **Plain** | 1.6951 | -0.324 | 3.8124 | -0.172 |
| **Turbo-BII HP** | 1.1453 | 0.037 | - | - |
| **High Flux** | 2.0508 | 0.234 | - | - |
| **Turbo-EDE2** | 0.8497 | -0.306 | 1.5650 | 0.135 |

**Prediction of Heat Transfer on a Single-Tube Row for Partially-Wet Conditions**. The heat transfer coefficient for the dry region $\alpha_{dry}$, that is for the natural convection, has a negligible contribution to the calculation of α for the entire surface of a partially-wet tube. Since $\alpha_{dry} << \alpha_{wet}$, the heat transfer coefficient can be simply expressed using a linear expression:

$$\alpha_{array} = F\,\alpha_{wet} \qquad [14.7.10]$$

In this expression, F represents the fraction of the tube surface covered by liquid. Their new method for prediction of F is a simple linear relationship with respect to $Re_{onset}$, taking into account both the heat flux and fluid property effects:

$$F = \begin{cases} Re_{top}/Re_{onset} & \text{for } Re_{top} < Re_{onset} \\ 1 & \text{for } Re_{top} \geq Re_{onset} \end{cases} \qquad [14.7.11]$$

For the all wet condition, when $Re_{top} \geq Re_{onset}$, F = 1.0; otherwise F < 1.0 and decreases the heat transfer coefficient. This method is simple to use and is based on $Re_{onset}$ calculated at each heat flux. No additional empirical constant is needed to obtain the value of F. Hence, in their new method only two fluid/tube specific empirical constants are required, much fewer than before but still not a general expression applicable without experimental single-row test data available.

Table 14.4 shows their method's accuracy versus a selection of tubes, citing the percent of the predicted values within ±30% of the corresponding measured values (the uncertainty of the experimental value is

also shown for comparison). As the prediction method will in practice be primarily applied to all wet data, the prediction accuracies of the local heat transfer coefficients for partially-wet and all wet conditions are segregated in Table 14.5 within a ±20% interval. As can be seen, the method works quite well for the all wet data, where the larger discrepancies come from the very highly performing tubes for which the experimental uncertainties are larger than the ±20% interval.

**Table 14.4. Accuracy of the prediction method for all data (all wet plus partially-wet).**

| | R-134a | | R-236fa | |
|---|---|---|---|---|
| **Tube** | **all** | **uncertainty** | **all** | **uncertainty** |
| **Plain** | 89.9 ± 30% | 10 – 20% | 82.1 ± 30% | 15 – 25% |
| **Turbo-EDE2** | 77.6 ± 30% | 25 – 35% | 81.2 ± 30% | 25 – 30% |
| **Turbo-BII HP** | 90.7 ± 30% | 10 – 20% | - | - |
| **High Flux** | 72.2 ± 30% | 25 – 35% | - | - |

**Table 14.5. Accuracy of the prediction method for data segregated into partially-wet and all-wet data.**

| | R-134a | R-236fa | | |
|---|---|---|---|---|
| **Tube** | **partially-wet** | **all-wet** | **partially-wet** | **all-wet** |
| **Plain** | 61.2 ± 20% | 94.6 ± 20% | 28.9 ± 20% | 87.1 ± 20% |
| **Turbo-EDE2** | 35.6 ± 20% | 75.5 ± 20% | 34.2 ± 20% | 80.6 ± 20% |
| **Turbo-BII HP** | 36.1 ± 20% | 95.8 ± 20% | - | - |
| **High Flux** | 81.5 ± 20% | 30.3 ± 20% | - | - |

Direct comparison of the present method with other authors' data in the literature was not appropriate as those data are tube length averaged data (not local data), which may include local areas of dryout along part of the tube in the average, making it impossible to correctly analyze such data.

**Prediction of Heat Transfer on a Tube Bundle**. The falling film evaporation bundle results in Habert and Thome (2010a) were rather scattered because of: (*i*) a large error propagation on the measurements of such high heat transfer coefficients and (ii) the liquid maldistribution within the tube bundle that induced prematurely tripping the onset of dryout for some tubes by creating a bypass around some tubes but not others. Due to this, the prediction method proposed in Habert and Thome (2010b) was restricted to only their data for the top three tubes, as they are less affected by any non-ideal liquid distribution and performed relatively well. The typical bundle effect they observed on these three tubes is shown schematically in Figure 14.23: with decreasing film Reynolds number for a film flowing from the top of a bundle towards the bottom, the heat transfer coefficient begins at a plateau corresponding to approximately the single-row array plateau value, then increases to a peak, then falls off again to the single-plateau value, and then falls off rapidly below the onset of dryout threshold. As it was not possible to identify the mechanism creating the peak, an empirical factor B was defined that satisfactorily predicts the results from their database as follows:

$$\alpha_{bundle} = B\,\alpha_{array} \qquad [14.7.12]$$

$$B = 1 + e \cdot \exp(-f(Re_{top} - Re_{peak})^2 \qquad [14.7.13]$$

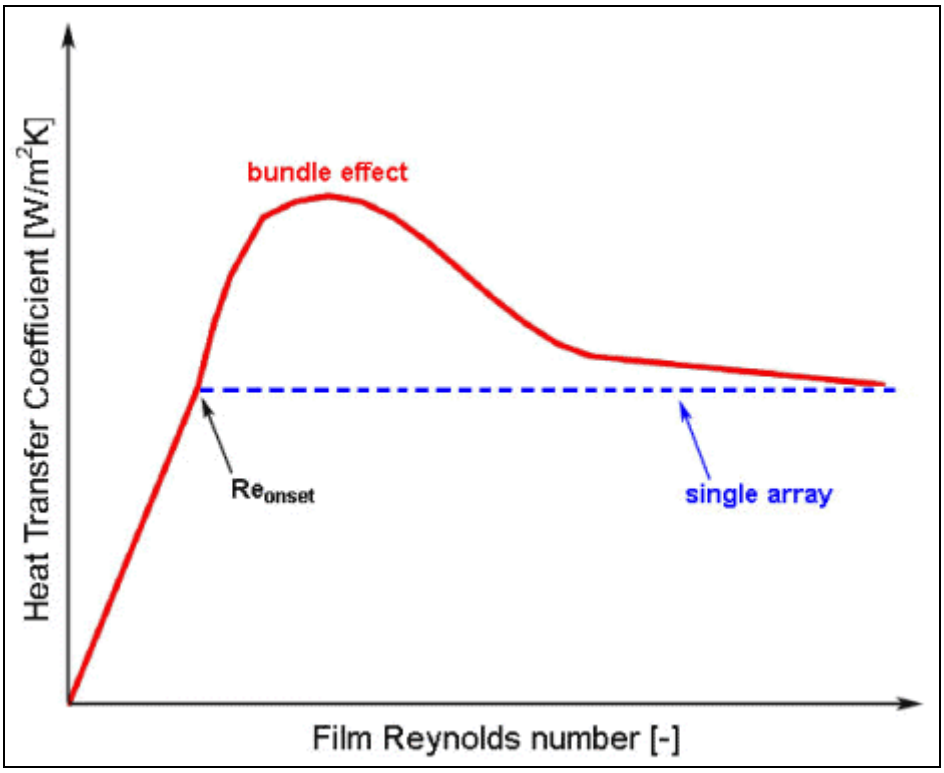


**Figure 14.23. Heat transfer trends observed for falling film evaporation on the first three rows of the tube bundle of Habert and Thome (2010b).**

This approach was applied with limited success to the plain tube results for all the database excluding the R-236fa results at 60kW/m$^2$, in which almost all the tubes were partially-wet or nearly completely dry. Table 14.6 shows the values of e, f and $Re_{peak}$ for the plain tube. The method predicts both partially-wet and wet data reasonably well. The bundle factor satisfactorily predicts the peak and the subsequent decrease in heat transfer coefficient. Predicting the partially-wet data becomes less precise when increasing the heat flux, due to an increase in bubble generation causing premature local dryout. The single array prediction method (B = 1) was used for the R-134a data at 60 kW/m$^2$, giving good prediction of the wet data. This suggests that the bundle effect tends to disappear with increasing heat flux. Future tests with more extensive data and flow visualization are required for refinement of the method and the physics of the flow.

**Table 14.6. Empirical constants e and f and the value of $Re_{peak}$ for the plain tube bundle prediction.**

| | R-134a | | | R-236fa | | |
|---|---|---|---|---|---|---|
| **Heat Flux** | **e** | **f** | **$Re_{peak}$** | **e** | **f** | **$Re_{peak}$** |
| **20kW/m$^2$** | 0.6 | 9 $10^{-7}$ | 800 | 0.8 | 4 $10^{-7}$ | 600 |
| **40kW/m$^2$** | 0.2 | 9 $10^{-7}$ | 1000 | 0.3 | 4 $10^{-7}$ | 800 |

Due to the higher propagation of error on the very large heat transfer coefficients for the Turbo-EDE2 tubes, only tubes 1 and 2 could be correlated as they are the less disturbed by the non-uniformity of the liquid flow experienced on the lower tubes. For these tubes, the range of film Reynolds numbers tested was not wide enough to characterize the onset of dryout. For these all wet data, the heat transfer

performance had little influence from the film Reynolds number (similar to this tube's single-row data), and thus the bundle factor B becomes simply a non-unity constant. Table 14.7 gives the values of the bundle factor B at different heat flux conditions with their respective precision (% of data points within the indicated error interval). Interestingly, B = 1.1 for three of the four cases. Furthermore, it is interesting to note that with B = 0.6, this effectively degrades the bundle performance with respect to the single-array results by 40% while with B = 1.1 it increases performance by 10%. Their bundle method presented here is to taken as a preliminary method that requires more experimental tests that includes flow visualization to investigate the flow maldistribution problem that leaves some tubes unexpectedly partially dry.

**Table 14.7. Empirical constant B for the Turbo-EDE2 bundle.**

| | R-134a | | R-236fa | |
|---|---|---|---|---|
| **Heat Flux** | **B** | **Precision** | **B** | **Precision** |
| **40 kW/m$^2$** | 1.1 | 94.5% in ± 5% | 1.1 | 88.9% in ± 20% |
| **60 kW/m$^2$** | 0.6 | 87.5% in ± 10% | 1.1 | 73.5% in ± 20% |

Summarizing, most existing falling film evaporation prediction methods, including those above, have a quite limited range of application because they require empirical parameters obtained from experimental tests to finalize the prediction method. Furthermore, most have been developed using data for only one or two fluid/surface combination(s) at one test pressure, making their application to other situations only a qualitative guess. On the other hand, there is no general method yet for predicting falling film evaporation heat transfer coefficients and the methods noted above are applicable to R-134a for several types of tubes at the typical operation saturation temperature of 5°C.

## 14.8 SUMMARY

Falling film heat transfer under evaporating conditions is controlled by two heat transfer mechanisms: (i) the evaporating film coefficient for heat conduction and/or convection of heat through the film to the interface, and (ii) the nucleate boiling heat transfer coefficient if present in the film. Film evaporation creates vapor at the interface of the liquid film while nucleate boiling evaporates liquid within the film itself. The evaporating film coefficient can be for a thermally developing flow at the top of the horizontal tube or for a fully developed flow. The film flow can be either laminar or turbulent with or without interfacial ripples. Nucleate boiling is only present if the heat flux threshold for onset of nucleate boiling has been surpassed. Intense nucleate boiling in the film can also cause premature formation of dry patches on the surface.

Experimental heat transfer data for numerous horizontal single-tube and small horizontal tube bundles have measured for numerous fluids, such as water, iso-propanol, ethylene glycol, and refrigerants R-12, R-22, R-113, R-123 (plus oil), R-134a (plus oil), and R-717 (ammonia). These studies covered plain tubes, low finned tubes, enhanced boiling tubes and enhanced condensation tubes. Most tests were for single-tubes but some were also performed for small tube bundles.

For refrigerant R-134a and R-123 applications, the principal interest is in enhanced tube performance. Some enhanced condensation surfaces performed very well, such as the Turbo-Cii, while some enhanced boiling tubes performed better under falling film conditions with nucleate boiling in the film compared to their original pool boiling curves. The influence of oil was to increase heat transfer significantly in most cases, even for the enhanced tubes; however this positive effect tended to diminish with increasing heat flux.

The influences of film feed rate, heat flux, enhancement geometry effects, staggered or inline tube layouts, tube pitch, tube diameter, nozzle type and height above the bundle, saturation temperature, oil concentration, etc. have been investigated for heat transfer and film flow modes between tube rows. All of these are important factors in the heat transfer process and require further study before useful design guidelines can be proposed.

Numerous design methods have been proposed for falling film evaporation, with and without nucleate boiling in the film, for plain tubes. In addition, methods for identifying flow modes between vertical tube rows on plain tube and enhanced tube bundles have been developed. Heat transfer correlations for subcooled falling liquid films (i.e. without evaporation) flow down a vertical array of horizontal tubes have been proposed. A selection of these methods has been presented here. These methods so far can only predict a few of the influences of the above mentioned parameters on thermal performance and few of these proposed methods have been validated against independent data sets and none against sizable databases.